

PROCESS-ORIENTED GEOMETRIC SINGULAR PERTURBATION THEORY AND CALCIUM DYNAMICS

SAMUEL JELBART*, NATHAN PAGES†, VIVIEN KIRK†, JAMES SNEYD†, AND MARTIN WECHSELBERGER‡

Abstract. Phenomena in chemistry, biology and neuroscience are often modelled using ordinary differential equations (ODEs) in which the right-hand-side is comprised of terms which correspond to individual ‘processes’ or ‘fluxes’. Frequently, these ODEs are characterised by multiple time-scale phenomena due to order of magnitude differences between contributing processes and the presence of *switching*, i.e., dominance or sub-dominance of particular terms as a function of state variables. We outline a heuristic procedure for the identification of small parameters in ODE models of this kind, with a particular emphasis on the identification of small parameters relating to switching behaviours. This procedure is outlined informally in generality, and applied in detail to a model for intracellular calcium dynamics characterised by switching and multiple (more than two) time-scale dynamics. A total of five small parameters are identified, and related to a single perturbation parameter by a polynomial scaling law based on order of magnitude comparisons. The resulting singular perturbation problem has a time-scale separation which depends on the region of state space. We prove the existence and uniqueness of stable relaxation oscillations with three distinct time-scales using a coordinate-independent formulation of GSPT in combination with the blow-up method. We also provide an estimate for the period of the oscillations, and consider a number of possibilities for their onset under parameter variation.

Key words. intracellular calcium dynamics, non-standard geometric singular perturbation theory, switching, multiple time-scales, relaxation oscillations, blow-up

AMS subject classifications. 34C15, 34C26, 34E15, 37N25, 92C37

1. Introduction. Chemical, biological and physiological phenomena are often modelled by systems of ordinary differential equations (ODEs) which contain multiple time-scales. This is a natural consequence of the fact that the underlying chemical, biological or physiological processes relevant to the dynamics naturally operate on time-scales which can span several orders of magnitude. Singular perturbation theory provides a mathematical toolbox for the analysis of multi-scale problems of this kind. In particular, many authors have demonstrated the suitability of *geometric singular perturbation theory (GSPT)* [10, 29, 18, 47] in combination with a method of geometric desingularization known as *blow-up* [8, 26, 27] as a rigorous and geometrically informative framework for the analysis of such problems; see [19, 20, 37] for examples in mathematical chemistry, [6, 43, 38, 42, 46] for examples in mathematical neuroscience, and [21, 24, 30] for examples in the context of biological and physiological systems.

Despite the success of these analyses, however, for many multi-scale ODEs arising in applications there are still a number of significant modelling and analytical obstacles to be overcome. For example, a necessary pre-condition for the formulation of an ODE as a perturbation problem, and hence for an analysis via GSPT, is the identification of a suitable perturbation parameter $\epsilon \ll 1$. In many systems of interest, there is no explicit perturbation parameter ϵ , and the modeller is confronted with the problem of how to introduce an ϵ without compromising the validity of the model. The opposite problem is also common, i.e., many applications feature multiple candidates for small parameters. In this case, the modeller is often forced to choose which (if any) of the candidate small parameters should be considered as ‘relevant’ perturbation parameter(s). In the case of more than one perturbation parameters, the ordering or relation between these ‘ ϵ ’s becomes significant for the validity and tractability of the resulting perturbation problem. Furthermore, models of this type are often characterised by additional analytical problems stemming from the presence of many time-scales [20, 25], non-trivial time-scale separations depending on the region of state and/or parameter space [47, 33, 21, 19, 25, 13], and ‘switching’, i.e., convergence to a non-smooth singular limit as a perturbation parameter tends to zero [21, 24, 40, 16, 36, 11].

In recent years, significant progress towards overcoming these analytical obstacles has been made by

*Department of Mathematics, University of Munich, Garching. jelbart@ma.tum.de, partially supported through the SFB/TRR 109 Discretization and Geometry in Dynamics grant and the Australian Research Council grant DP180103022.

†Department of Mathematics, University of Auckland, Auckland. npag780@aucklanduni.ac.nz, v.kirk@auckland.ac.nz, sneyd@math.auckland.ac.nz, partially supported by grant 15-UOA-184 of the Marsden Fund of the Royal Society of New Zealand.

‡School of Mathematics & Statistics, University of Sydney, Sydney. martin.wechselberger@sydney.edu.au, partially supported through Australian Research Council grant DP180103022.

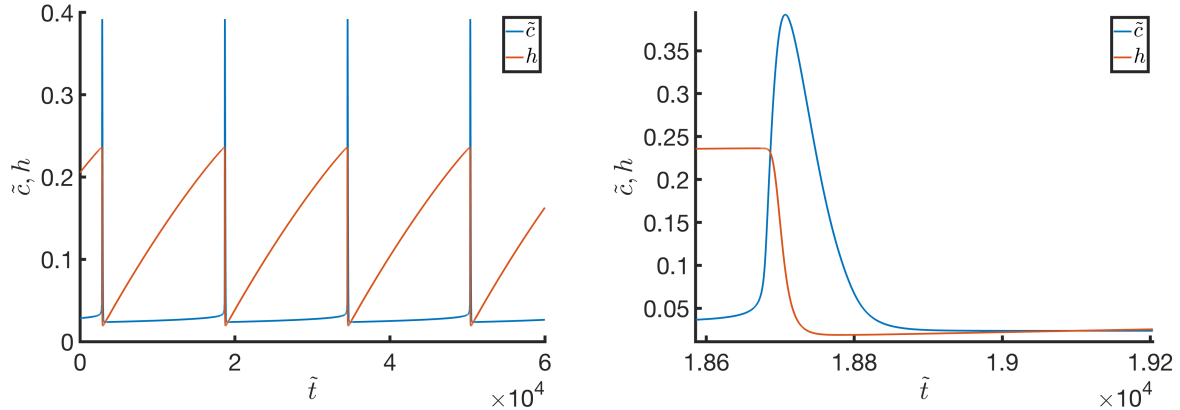


Fig. 1: Relaxation oscillations in a model for intracellular calcium dynamics defined in Section 3, system (4.2). Left: time series for the two state variables \tilde{c} and h . Right: enlargement of one spike. Both \tilde{c} and h exhibit multiple time-scale dynamics, indicative of a non-standard time-scale separation.

many authors. In [47], a coordinate-independent framework for GSPT which is applicable for systems with time-scale separations depending on the region of state space is outlined in detail. Such a framework has also been developed and applied successfully to models for chemical reactions in, for example, [12, 13], and previous work by Szmolyan et al [19, 21, 24] demonstrates that GSPT and blow-up techniques are well suited to analyses of problems of this kind. In [20] the authors successfully analysed a model for glycolytic oscillations featuring multiple small parameters and more than two time-scales using GSPT and blow-up techniques. In [5] the GSPT framework was extended to account for any number of small parameters and time-scales, similar results in the more general case with no assumed separation of fast/slow variables have been developed and applied in [25], and in [32] progress is made towards the identification and analysis of so-called ‘hidden time-scales’ in such systems. In [21] the authors demonstrate that GSPT and blow-up techniques can be adapted to study problems characterised by ‘switching’, a common feature of ODE models in mathematical biology due, for example, to the rapid activation or inactivation of certain processes once a threshold agonist or chemical concentration is reached. Finally, the authors in [24] were able to show that blow-up techniques developed originally for the study of regularised (smoothed) piecewise-smooth systems [4, 34, 35, 22, 23] can be used in order analyse these systems using singular perturbation theory.

Our aim in this work is to develop a heuristic procedure for the derivation and analysis of such perturbation problems, focusing in particular on models without *a priori* knowledge of relevant perturbation parameters. In light of the significant progress toward overcoming the analytical problems associated with singular perturbation analysis outlined in the preceding paragraph, emphasis is placed here on the identification of small parameters and reformulation of a model as a singular perturbation problem. This procedure is outlined in generality, but developed primarily via application to a model of intracellular calcium oscillations [45]. Although the model is only two-dimensional, it features many of the obstacles discussed above and therefore serves as a suitable case study for the development of our methods. Figure 1 shows numerical evidence of relaxation oscillations with two or more time-scales in the model, with a time-scale separation which depends on the region of state space. This is evident by the presence of fast and slow components in both state variables. The model also exhibits switching, i.e., sharp dynamical transitions caused by the fact that some of the model fluxes change quickly, in a threshold-like fashion, as the calcium concentration changes. Applying our heuristic procedure to the model, we identify multiple small parameters, which are then linked to a single small parameter via a suitable polynomial scaling based on order of magnitude comparisons. We then prove existence, uniqueness and stability of the observed relaxation oscillations in the singular perturbation problem derived via our methods, provide an estimate for the period of the oscillations, and consider a number of mechanisms for their onset under parameter variation.

The manuscript is structured as follows. In Section 2 we outline the general procedure for deriving a suitable singular perturbation problem. In Section 3 we present the model from [45] and its reduction to the closed-cell form we will analyze. In Section 4 we apply our procedure to the (closed-cell) calcium model, and derive the corresponding singular perturbation problem. Section 5 is devoted to a GSPT analysis of this system, including the statement of our main results. The detailed blow-up analysis required to prove existence of the relaxation oscillations, as well as the bifurcation analysis of the model, is deferred to the Appendix for expository reasons. In Section 6 we summarise and conclude.

2. Outline of the method. In the following we outline our heuristic procedure for deriving singular perturbation problems from ODE models characterised by multi-scale and/or switching behaviour.

Given a model expressed as a system of ODEs comprised of identifiable process/flux terms, perform the following steps:

- (I) *Non-dimensionalise.* This is crucial for revealing the relative magnitudes and time-scales associated with particular process/flux terms.
- (IIa) *Associate small parameters to maximal process/flux rates.* Following step (I), each process/flux term can be written as the product of a constant scaling factor and a normalised process/flux term. Numerically ‘small’ scaling factors constitute candidates for small parameters $\epsilon_i \ll 1$.
- (IIb) *Associate small parameters to steep switches in process/flux terms.* Identify sources of ‘steep’ switching and associated candidate small parameters $\epsilon_i \ll 1$ such that the limit $\epsilon_i \rightarrow 0$ yields an approximation by a non-smooth switch.
- (III) *Relate small parameters.* Use numerical order of magnitude comparisons to relate candidate small parameters identified in (IIa) and/or (IIb). Choose a polynomial scaling with respect to a single small parameter ϵ as follows: for $i = 1, \dots, m$ small parameters ϵ_i we have

$$(2.1) \quad \epsilon = a_1 \epsilon_1^{b_1} = a_2 \epsilon_2^{b_2} = \dots = a_m \epsilon_m^{b_m},$$

where ϵ_i are the candidate small parameters from (IIa) and (IIb), the a_i are of numerical order 1 and the exponents $b_i > 0$. There should exist a fixed numerical value of $\epsilon \ll 1$ such that the original (dimensionless) parameter values, i.e., the actual parameter values prior to the scaling (2.1), are returned by setting ϵ equal to this number.

- (IV) *Analyse the system via perturbation theory.* If successful, steps (I)-(III) yield a well-defined system which can be analysed via the limiting (potentially non-smooth) dynamics.

Steps (I)-(III) provide a semi-systematic pre-processing of any dimensional (ODE) model for deriving a candidate perturbation problem, and will be carried out in detail for a model for intracellular calcium dynamics in Section 4. Step (IV), the analysis of the resulting perturbation problem, is presented for this case study in Section 5.

In the following we provide several remarks on the general procedure outlined above.

Remark 2.1. The procedure is developed and intended for application to ODE models exhibiting multi-scale and/or switching dynamics, and is expected to be of most use in this particular setting. In the case that a model has no clear multi-scale or switching behaviour, the procedure should output either a ‘null result’ in which no perturbation parameters are identified, or a regular perturbation problem, in which only small parameters that are not related to multi-scale structure or switching are identified. In the latter case the procedure still provides a simplification, even in the absence of multi-scale dynamics. In case of a singular perturbation problem, small parameters are identified in (IIa) only, in (IIb) only or in (IIa) and (IIb).

Remark 2.2. As always in applied settings, what constitutes a ‘sufficiently small’ numerical value for a parameter to be considered as a perturbation parameter in step (IIa) is debatable, and left to the discretion of the modeller. Typically, assertions that a particular value is ‘sufficiently small’ for the application of perturbation methods need to be justified in terms of agreements with numerical and/or experimental findings.

Remark 2.3. Similarly to the issues described in Remark 2.2 above, the question of whether or not a switch is ‘sufficiently steep’ to justify approximation by a non-smooth switch in step (IIb) is left to the

Parameter	Value	Units	Parameter	Value	Units
k_β	0.4	-	p	0.05	μM
K_c	0.2	μM	K_τ	0.1	μM
K_h	0.08	μM	V_s	0.9	μMs^{-1}
K_p	0.2	μM	K	0.00001957	-
k_{IPR}	10	s^{-1}	K_s	0.2	μM
τ_{max}	1000	s	γ	5.5	-
c_t	2	μM	-	-	-

Table 1: Default (dimensional) parameter values for the model, equations (3.3).

discretion of the modeller. A quantitative comparison can be seen by noting that in this case, the slope of the normalised switch should be ‘sufficiently large’ for the validity of such approximations. Such approximations should be motivated on numerical, experimental or analytical grounds (or a combination thereof), and subsequently justified in terms of agreement with numerical and/or experimental findings.

Remark 2.4. There are many ways in which one could choose to order or relate the identified small parameters. The choice to do so in a polynomial fashion as in step (IV) equation (2.1) is made for simplicity, and in some sense defines our method. It is also important to keep in mind for a given application whether some limits need to remain independent.

Remark 2.5. A singular perturbation problem with small parameters identified in step (IIa) may or may not be given in the so-called ‘standard form’, i.e it may or may not feature a separation of fast/slow variables. The identification of one or more perturbation parameters associated to switching in step (IIb), implies that the resulting perturbation problem loses smoothness at some order in the singular limit $\epsilon \rightarrow 0$. In this case, the system is generically ‘non-standard’, in the sense that it cannot be written in the standard form.

3. The model. In this section we introduce the model for intracellular calcium dynamics which will serve as a non-trivial case study for our approach. We consider the following model developed in [45]:

$$(3.1) \quad \begin{aligned} \tau_h(c) \frac{dh}{dt} &= h_\infty(c) - h, \\ \frac{dc}{dt} &= J_{\text{IPR}}(h, c, c_e) - J_{\text{SERCA}}(c, c_e) + J_{\text{pm}}(c), \\ \frac{dc_e}{dt} &= \gamma(J_{\text{SERCA}}(c, c_e) - J_{\text{IPR}}(h, c, c_e)), \end{aligned}$$

where c denotes the calcium concentration in the cytosol, c_e the calcium concentration in the endoplasmic reticulum (ER), and h is a gating variable describing the capacity of the IP_3 receptors (IPR) to allow the passage of calcium. The particular form of the fluxes $J_{\text{IPR}}(h, c, c_e)$, $J_{\text{SERCA}}(c, c_e)$, $J_{\text{pm}}(c)$ and the functions $h_\infty(c)$, $\tau_h(c)$ will be specified below. The parameter γ is the ratio between the volume of the cytosol and the volume of the ER. Default parameter values used in the model are specified in Table 1.

It is useful to define $c_t := c + c_e/\gamma$, which represents the total moles of free calcium in the ER and the cytosol, divided by the cytoplasmic volume. This variable can be used as an alternative to c_e in the model, yielding

$$(3.2) \quad \begin{aligned} \tau_h(c) \frac{dh}{dt} &= h_\infty(c) - h, \\ \frac{dc}{dt} &= J_{\text{IPR}}(h, c, c_t) - J_{\text{SERCA}}(c, c_t) + J_{\text{pm}}(c), \\ \frac{dc_t}{dt} &= J_{\text{pm}}(c), \end{aligned}$$

where by replacing the argument c_e by c_t in the flux terms $J_{\text{IPR}}(h, c, c_t)$ and $J_{\text{SERCA}}(c, c_t)$ we have permitted a slight abuse of notation. The flux term $J_{\text{pm}}(c)$ represents the exchange of calcium between the cytosol and

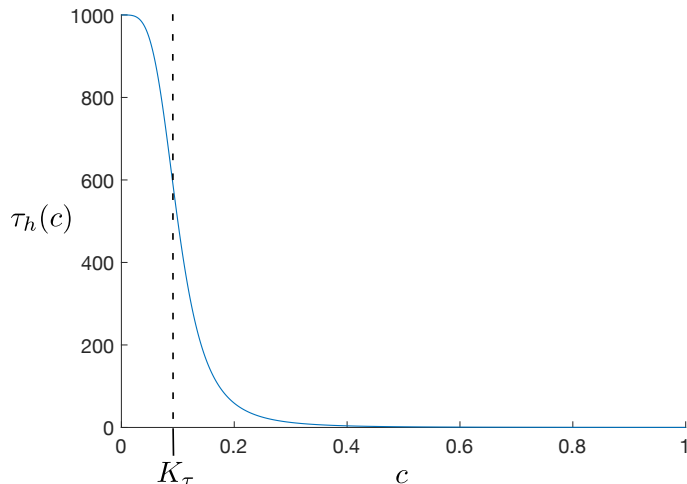


Fig. 2: The function $\tau_h(c)$ defined in (3.4) varies over several orders of magnitude with c , which causes the speed of evolution of h to vary significantly through state space.

the extracellular medium. This calcium efflux is typically slow compared to the rate of other calcium fluxes in the cell and is not necessary on either physiological [3] or mathematical [39] grounds in order for there to be oscillations. Blocking the $J_{\text{pm}}(c)$ flux term obtained by setting $J_{\text{pm}}(c) \equiv 0$ gives the corresponding *closed-cell model*. The study of this reduced model gives enormous insight into the behaviour of the full model, and thus a closed-cell analysis is an important first step for the analysis of almost any model of intracellular calcium. The closed-cell reduction leads to a planar system:

$$(3.3) \quad \begin{aligned} \tau_h(c) \frac{dh}{dt} &= h_\infty(c) - h, \\ \frac{dc}{dt} &= J_{\text{IPR}}(h, c) - J_{\text{SERCA}}(c), \end{aligned}$$

where the total calcium c_t is now a parameter. In this work, we focus on understanding the dynamics of the closed-cell model (3.3).

We now specify the functional form of $\tau_h(c)$ and the flux terms. The functions $\tau_h(c)$ and $h_\infty(c)$ are given by Hill functions

$$(3.4) \quad \tau_h(c) = \tau_{\text{max}} \frac{K_\tau^4}{K_\tau^4 + c^4}, \quad h_\infty(c) = \frac{K_h^4}{K_h^4 + c^4},$$

which are monotonically decreasing switch-like functions; see Figure 2. Note that due to the constant factor τ_{max} , the value of $\tau_h(c)$ in particular varies between 0 s and 1000s depending on c . This induces a sharp, switch-like variation in the speed of evolution of h as a function of calcium concentration c .

J_{IPR} represents the flux of calcium from the ER to the cytosol through the IPR, and is modelled by

$$(3.5) \quad J_{\text{IPR}}(h, c) = \gamma k_{\text{IPR}} P_O(h, c) (c_t - (1 + 1/\gamma)c),$$

where k_{IPR} is the maximum flux through the IPR and P_O is the open probability of the IPR. There are numerous models for P_O in the literature [9, 44, 41, 1]. Here we adopt the form proposed in [45], which is one of the simplest and most recent. We set

$$(3.6) \quad P_O(h, c) = \frac{\beta(h, c)}{\beta(h, c) + k_\beta (\beta(h, c) + \alpha(c))},$$

Parameter	Value	Parameter	Value
\tilde{k}_β	0.4	\tilde{K}_τ	0.05
\tilde{K}_c	0.1	\tilde{V}_s	0.0081
\tilde{K}_s	0.1	\tilde{K}	0.000019
\tilde{K}_p	0.1	\tilde{K}_h	0.04
\tilde{k}_{IPR}	0.18	γ	5.5
\tilde{p}	0.025	$\tilde{\tau}_{\text{max}}$	55000
\tilde{c}_t	1	-	-

Table 2: Dimensionless parameters in system (4.2). The tilde notation is dropped in step (IIa).

where

$$\alpha(c) = \phi_{pdown}(1 - m_\alpha(c)h_\infty(c)), \quad \beta(h, c) = \phi_p m_\alpha(c)h,$$

with Hill-type functions

$$m_\alpha(c) = \frac{c^4}{K_c^4 + c^4}, \quad \phi_{pdown} = \frac{K_p^2}{K_p^2 + p^2}, \quad \phi_p = \frac{p^2}{K_p^2 + p^2}.$$

Finally, J_{SERCA} is the flux from the cytosol to the ER via the ATPase pumps. The SERCA pump model is bidirectional, and given by

$$(3.7) \quad J_{\text{SERCA}}(c) = V_s \frac{c^2 - K\gamma^2(c_t - c)^2}{K_s^2 + c^2} = J_{\text{SERCA}}^+(c) - J_{\text{SERCA}}^-(c),$$

where

$$J_{\text{SERCA}}^+(c) = V_s \left(\frac{c^2}{K_s^2 + c^2} \right), \quad J_{\text{SERCA}}^-(c) = K\gamma^2 V_s \left(\frac{(c_t - c)^2}{K_s^2 + c^2} \right).$$

The decomposition into two separate terms J_{SERCA}^\pm reflects the fact that J_{SERCA} models two separate fluxes: one positive, resulting from calcium ions being pumped from the cytosol to the ER, and one negative, corresponding to a leak of calcium ions from the ER into the cytosol.

The model (3.3) has parameters spanning multiple orders of magnitude (see Table 1), as well as multiple Hill-type functions which induce a nonlinear switching behaviour as a function of calcium concentration c . Both features can potentially lead to a (possibly hidden) multiple time-scale structure. Our aim in the next section is to reveal any multiple time-scale structure by applying the procedure outlined in Section 2.

4. Deriving a singular perturbation problem. In this section, we apply steps (I)-(III) to the calcium model (3.3) in order to derive a system amenable for an analysis using perturbation methods.

Step (I): Non-dimensionalise. We begin by non-dimensionalising the model (3.3). As well as making the variables unitless, this process also rescales the variables to ensure they are of order one for the regions of state and parameter space of interest. Since $h \in [0, 1]$ is already dimensionless, we only need to non-dimensionalise the variables c and t . We define

$$(4.1) \quad c = Q_c \tilde{c}, \quad t = T \tilde{t},$$

where Q_c and T denote a reference concentration and time-scale respectively, to be specified below.

We obtain the following dimensionless model:

$$(4.2) \quad \begin{aligned} \tilde{\tau}_h(\tilde{c}) \frac{dh}{d\tilde{t}} &= \tilde{h}_\infty(\tilde{c}) - h, \\ \frac{d\tilde{c}}{d\tilde{t}} &= \tilde{J}_{\text{IPR}}(h, \tilde{c}) - \tilde{J}_{\text{SERCA}}(\tilde{c}), \end{aligned}$$

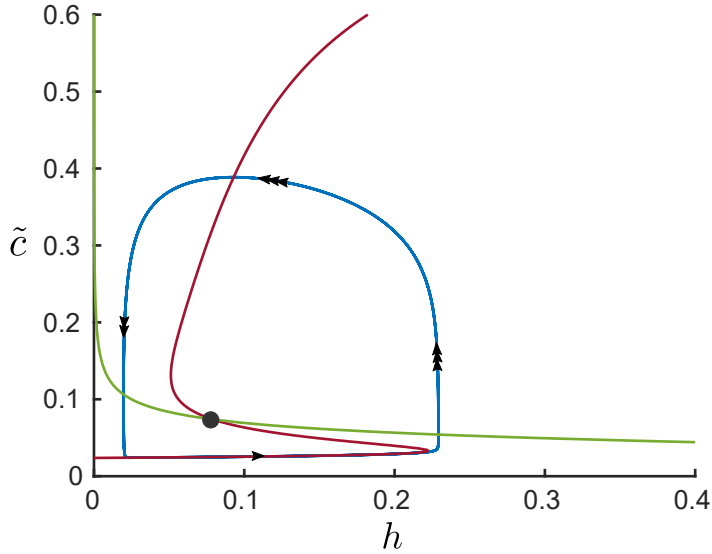


Fig. 3: State space representation of the relaxation oscillations in system (4.2) with parameter values from Table 2, c.f. the corresponding time series in Figure 1. The $\tilde{c}' = 0$ and $h' = 0$ nullclines are shown in red and green respectively, and the unique equilibrium corresponding to their intersection is indicated by a black disk. Notice that the limit cycle closely follows the $\tilde{c}' = 0$ nullcline near the h axis, indicative of multiple time-scale dynamics. Curvature in the phase of the limit cycle bounded away from the nullclines is indicative of a non-standard time-scale separation, since both h and \tilde{c} are fast in this regime. The relative speed of the oscillation about the limit cycle is indicated by single, double and triple arrows. Note that the downward motion (approximately parallel to the \tilde{c} -axis) is faster than the motion along the $\tilde{c} = 0$ nullcline, but slower than the ‘upward’ and ‘leftward’ components of the oscillation; see again Figure 1b.

where the new (dimensionless) expressions $\tilde{\tau}_h(\tilde{c})$, $\tilde{h}_\infty(\tilde{c})$, $\tilde{J}_{\text{IPR}}(h, \tilde{c})$ and $\tilde{J}_{\text{SERCA}}(\tilde{c})$ are defined analogously to their dimensional counterparts, except in terms of the new (dimensionless) parameters

$$(4.3) \quad \tilde{K}_i = \frac{K_i}{Q_c}, \quad \tilde{\tau}_{\max} = \frac{\tau_{\max}}{T}, \quad \tilde{k}_{\text{IPR}} = T k_{\text{IPR}}, \quad \tilde{V}_s = \frac{T}{Q_c} V_s, \quad \tilde{c}_t = \frac{c_t}{Q_c}, \quad \tilde{p} = \frac{p}{Q_c},$$

where $i = c, h, \tau, s$ or p . We choose the following reference scales for our model:

$$(4.4) \quad Q_c = c_t = 2, \quad T = \frac{1}{\gamma k_{\text{IPR}}} = \frac{1}{55}.$$

Thus, (4.2) shows the dynamics of c relative to the total concentration c_t , on the IPR time-scale set by the uniform scaling γk_{IPR} ; this is the fastest time-scale in the system. Numerical values for the dimensionless model parameters consistent with Table 1 are shown in Table 2. The relaxation oscillations in Figure 1 were computed using system (4.2) with the (dimensionless) parameters in Table 2. The multiple time-scale structure is also reflected in state space, see Figure 3. The presence of curvature in the ‘fast part’ of the limit cycle bounded away from the nullclines reflects the fact that both h and \tilde{c} are ‘fast’ in this regime, indicating a non-standard time-scale separation.

In what follows we refer only to the dimensionless model (4.2) and parameters (4.3), dropping the tildes for notational simplicity.

Step (IIa): Associate small parameters to maximal process/flux rates. Consider the dimensionless system (4.2). We need to compare relative magnitudes of the constant scaling factors associated to

the (dimensionless) flux terms. These are given by

$$(4.5) \quad \frac{1}{\tau_{\max}} = 1.8 \times 10^{-5}, \quad \gamma k_{\text{IPR}} = 1.0, \quad V_s = 8.1 \times 10^{-3}, \quad \frac{V_s K \gamma^2 K_s^2}{c_t^2} = 4.7 \times 10^{-8},$$

using the parameter values in Table 2. Note that the largest scaling factor is $\gamma k_{\text{IPR}} = 1.0$ due to the choice of non-dimensionalisation in step (I). Based on these order of magnitude comparisons, we introduce three candidate small parameters:

$$(4.6) \quad \epsilon_1 = \frac{1}{\tau_{\max}}, \quad \epsilon_2 = V_s, \quad \epsilon_3 = \frac{V_s K \gamma^2 K_s^2}{c_t^2}.$$

Note that at this point, the ϵ_i are considered to be independent. Their magnitudes relative to each other will be considered in step (III).

Introducing the small parameters ϵ_i , we obtain the system

$$(4.7) \quad \begin{aligned} \left(\frac{\tau_h(c)}{n_h} \right) h' &= \epsilon_1 (h_\infty(c) - h), \\ c' &= J_{\text{IPR}}(h, c) - \epsilon_2 \left(\frac{J_{\text{SERCA}}^+(c)}{n_{\text{SERCA}}^+} \right) + \epsilon_3 \left(\frac{J_{\text{SERCA}}^-(c)}{n_{\text{SERCA}}^-} \right), \end{aligned}$$

where $n_h = \tau_{\max}$, $n_{\text{SERCA}}^+ = V_s$ and $n_{\text{SERCA}}^- = V_s K \gamma^2 K_s^2 / c_t^2$ are the normalisation constants associated with $\tau_h(c)$, $J_{\text{SERCA}}^+(c)$ and $J_{\text{SERCA}}^-(c)$ respectively. Notice that by (4.6), we have

$$\epsilon_1 n_h = \frac{\epsilon_2}{n_{\text{SERCA}}^+} = \frac{\epsilon_3}{n_{\text{SERCA}}^-} = 1.$$

In the perturbation analysis which follows, we consider the limiting dynamics as $\epsilon_1, \epsilon_2, \epsilon_3 \rightarrow 0$ while keeping $n_h, n_{\text{SERCA}}^+, n_{\text{SERCA}}^-$ fixed. The basic modelling assumption is that the perturbation analysis for $\epsilon_1, \epsilon_2, \epsilon_3 \ll 1$ is valid and informative for values of $\epsilon_1, \epsilon_2, \epsilon_3$ up to the numerical values corresponding to equations (4.5) and (4.6).

Step (IIb): Associate small parameters to steep switches in process/flux terms. As observed in Section 3, the presence of the Hill function $\tau_h(c)$ in the left-hand-side of system (3.3) is expected to lead to significant time-scale variation in the h dynamics as a function of the calcium concentration c . However, this has not been accounted for in the introduction of small parameters ϵ_i in step (IIa). This can be seen by considering $\epsilon_i \rightarrow 0$ for each $i = 1, 2, 3$ in system (4.7). The system obtained in this (singular) limit fails to capture the structure of the oscillations identified in Figures 1 and 3. In particular, the resulting limiting problem has $h' = 0$, so its fast dynamics (vertical in c) cannot accurately represent the observed (fast, nonlinear) solution segment that occurs away from the c - and h -axes.

In order to understand the role of switching in the model (3.3), we consider the effect of the five Hill-type functions

$$(4.8) \quad \tau_h(c), \quad h_\infty(c), \quad m_\alpha(c), \quad J_{\text{SERCA}}^\pm(c).$$

Each (normalised) Hill function is plotted in Figure 4, and each one is a candidate for approximation by a non-smooth switch. There are many ways to make such approximations, and the ‘best’ choice may depend heavily on the problem at hand. For our particular model (3.3), we shall appeal to the fact that general Hill-type functions

$$(4.9) \quad \text{Hill}_{K_d}^+(c) = \frac{c^m}{K_d^m + c^m} \quad \text{or} \quad \text{Hill}_{K_d}^-(c) = \frac{K_d^m}{K_d^m + c^m},$$

with half-value K_d and exponent $m \in \mathbb{N}_+$ can be well approximated by a suitable one-sided switch, given a sufficiently small half-value $K_d \ll 1$. This is achieved directly via the limit $K_d \rightarrow 0$ since

$$(4.10) \quad \lim_{K_d \rightarrow 0} \text{Hill}_{K_d}^+(c) = \begin{cases} 1 & \text{if } c > 0, \\ 0 & \text{if } c = 0, \end{cases} \quad \text{and} \quad \lim_{K_d \rightarrow 0} \text{Hill}_{K_d}^-(c) = \begin{cases} 0 & \text{if } c > 0, \\ 1 & \text{if } c = 0. \end{cases}$$

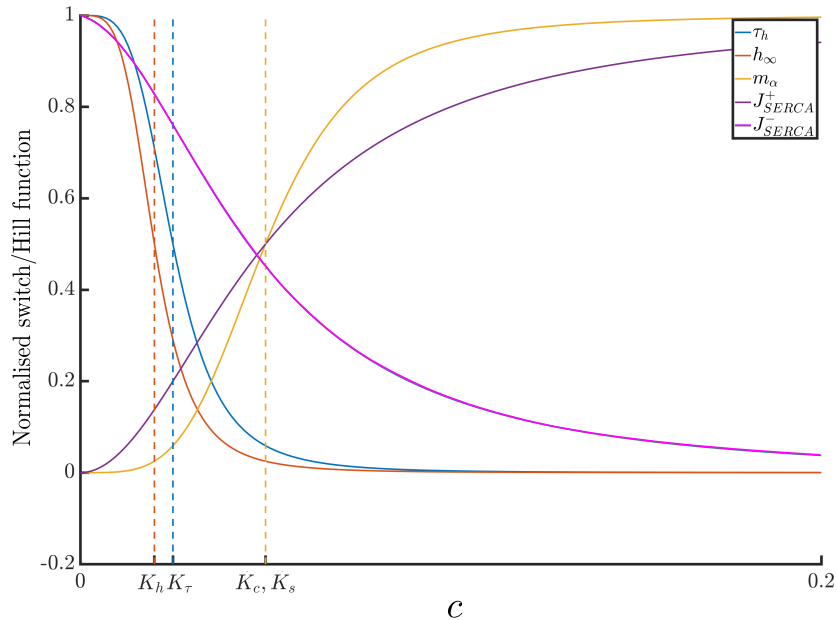


Fig. 4: Normalised switch-like functions in system (4.2), which play a role in determining the dominant processes in (4.2) for a given value of c . Corresponding half-values K_i for $i = h, \tau, c, s$ are also shown. The J_{SERCA}^- profile is less than 0.5 at the half-value K_s due to extra c_t -dependence in the numerator in (3.7). In order to derive a suitable perturbation problem from (3.3) we approximate the steepest of these, i.e. $\tau_h(c)$ and $h_\infty(c)$, by one-sided non-smooth switches via the limits in (4.10).

Such an approach has been used in [21] in the case of Michaelis-Menten terms (Hill functions (4.9) with $m = 1$), allowing for the detailed analysis of a non-standard relaxation oscillation in a minimal model of the embryonic cell cycle. In the following we consider which of the functions (4.8), if any, it is reasonable to approximate in this way.

Remark 4.1. Alternatively, one could obtain another non-smooth switch out of Hill-type functions (4.9) by fixing $K_d \in (0, 1)$ and taking the limit $m \rightarrow \infty$ where the discontinuity is located away from the boundary at $c = K_d$. See [40, 16, 36, 11] for examples of such an approach in the context of gene regulatory networks.

Making a limiting approximation of a smooth switch by a step function as in (4.10) is valid only for ‘sufficiently steep’ functions, i.e., the switch must exhibit a significant (order of magnitude or greater) variation over a ‘sufficiently narrow’ region in state space. As with the question “how small is small enough?”, the question “how steep is steep enough” is left to the discretion of the modeller, but can be informed by numerical and/or analytical considerations. A reasonable analytic approach is to adopt the notion that a switch may be considered (sufficiently) ‘steep’ if the magnitude of the derivative (i.e., the slope) evaluated at its midpoint is greater than 1 by a numerical order of magnitude, i.e., by at least a factor of 10. Calculating slopes for the switches in Figure 4, we find

$$(4.11) \quad \begin{aligned} \text{slope}(\tau_h)|_{K_\tau} &= 20, & \text{slope}(m_\alpha)|_{K_c} &= 10, & \text{slope}(h_\infty)|_{K_h} &= 25, \\ \text{slope}(J_{\text{SERCA}}^+)|_{K_s} &= 2.5, & \text{slope}(J_{\text{SERCA}}^-)|_{K_s \approx K_{mid}} &= 5.0. \end{aligned}$$

The large slopes associated to $\tau_h(c)$ and $h_\infty(c)$ suggest that they are suitable candidates for approximation by a non-smooth switch. Conversely, the slopes associated with the $J_{\text{SERCA}}^\pm(c)$ terms are still of numerical order 1, which suggests that these terms should not be analysed via non-smooth approximations. The question remains as to whether or not the slope associated with $m_\alpha(c)$ should be considered as sharp enough for the

validity of non-smooth approximations. In the following we shall adopt the principle that for borderline cases such as these additional approximations should be avoided; see however Remark 4.2 below. In accordance with this principle, we restrict ourselves to the non-smooth approximation of only the steepest Hill functions $\tau_h(c)$ and $h_\infty(c)$. We therefore introduce two more small parameters

$$(4.12) \quad \epsilon_4 = K_\tau, \quad \epsilon_5 = K_h.$$

The resulting perturbation problem will be given in step (III), once all five small parameters ϵ_i have been related to a single small parameter by a common scaling.

Remark 4.2. In general, additional (non-smooth) approximations can be expected to lead to simpler limiting systems, but the validity of the perturbation problem derived via these approximations as a means for studying the dynamics of the model (3.3) becomes harder to justify with each approximation. The aim is to balance tractability and accuracy, keeping in mind that one often comes at the expense of the other. In practice, a posteriori arguments will often also play an important role in striking such a balance. We have found for the model (3.3), that a non-smooth approximation of $\tau_h(c)$ and $h_\infty(c)$ alone is sufficient to capture the relevant dynamics in an analytically tractable way. However, one can continue to push for ‘more tractable’ perturbation problems describing the model (3.3) by introducing additional approximations. The next step, is to approximate $m_\alpha(c)$ by a non-smooth switch, followed by $J_{\text{SERCA}}^-(c)$, and so on. In general, this approximation procedure can be applied sequentially to each switch, starting with the steepest, and terminating at a point deemed by the modeller to strike the desired balance between accuracy and tractability.

Step (III): Relate small parameters. Steps (I)-(IIb) above yielded no fewer than five independent small parameters $\epsilon_i, i = 1, \dots, 5$. In order to obtain a tractable perturbation problem, we introduce a common scaling for all five ϵ_i in terms of a single small parameter ϵ . This can be achieved by defining ϵ in terms of one of the five ϵ_i and then determining sensible choices for the a_i and b_i in (2.1) based on order of magnitude comparisons for a fixed value of ϵ which returns the original parameter values in Table 2. We define a common small parameter ϵ via the choice

$$\sqrt{\epsilon} := \epsilon_4,$$

and the polynomial scaling

$$(4.13) \quad \epsilon := \epsilon_1^{1/2} \hat{\tau}_{\max}^{1/2} = \epsilon_2 \hat{V}_s^{-1} = \epsilon_3 \hat{K}^{-1} \gamma^{-2} = \epsilon_4^2 = \epsilon_5^2 \hat{K}_h^{-2}.$$

Equation (4.13) amounts to a choice of a_i and b_i in (2.1). Specifically, we have chosen exponents

$$b_1 = 1/2, \quad b_2 = 1, \quad b_3 = 1, \quad b_4 = 2, \quad b_5 = 2,$$

and coefficients a_i (which are defined in terms of the hatted parameters in (4.13)) which can be expressed in terms of the original (dimensionless) system parameters as follows:

$$(4.14) \quad a_1 = \hat{\tau}_{\max} = K_\tau^4 \tau_{\max}, \quad a_2 = \hat{V}_s = V_s K_\tau^{-2}, \quad a_3 = \hat{K} = K K_\tau^{-2}, \quad a_4 = 1, \quad a_5 = \hat{K}_h = K_h K_\tau^{-1}.$$

Notice that the a_i parameters $\hat{\tau}_{\max}, \hat{K}_h, \hat{V}_s$ and $\hat{K} \gamma^2$ are of numerical order 1 as required; see Table 3. Moreover, by setting $\epsilon = K_\tau^2 = 2.5 \times 10^{-3}$ and substituting the new rescaled parameter values from Table 3, the values coincide with the original parameter values in Table 2. Hence, for our particular problem, the assumption that the ϵ_i scale with a single ϵ according to (4.13) amounts to the assumption that $\epsilon = 2.5 \times 10^{-3}$ is ‘sufficiently small’ for the validity of perturbation arguments.

Remark 4.3. The choice to fix $\sqrt{\epsilon} = \epsilon_4$ was made a posteriori so that the leading order perturbation in the perturbation problem obtained is of order ϵ .

After applying the common scaling (4.13), we finally arrive at a version of the model in a form that is amenable to perturbation analysis, i.e., (4.15) defined in the following proposition.

Parameter	Value	Parameter	Value
k_β	0.4	ϵ	0.0025
K_c	0.1	\hat{V}_s	3.24
K_s	0.1	\hat{K}	0.0076
K_p	0.1	\hat{K}_h	0.8
k_{IPR}	0.18	γ	5.5
p	0.025	$\hat{\tau}_{\max}$	0.34
c_t	1	-	-

Table 3: Numerical parameter values for (4.15) and (4.18) obtained by setting $\epsilon = K_\tau^2 = 0.0025$ and applying (4.14) to the values of τ_{\max}, V_s, K in Table 2. All other parameter values are unchanged. The hat notation will be dropped in Section 5.

PROPOSITION 4.4. *System (4.2) can be written as*

$$(4.15) \quad \begin{aligned} h' &= \hat{\tau}_{\max}^{-1} (\mathfrak{h}_\infty(c, \epsilon) - h) (c^4 + \epsilon^2), \\ c' &= \mathfrak{J}_{IPR}(h, c, \epsilon) - \epsilon \mathfrak{J}_{SERCA}^+(c, \epsilon) + \epsilon^2 \mathfrak{J}_{SERCA}^-(c, \epsilon), \end{aligned}$$

where

$$(4.16) \quad \mathfrak{h}_\infty(c, \epsilon) = \frac{\epsilon^2 \hat{K}_h^4}{\epsilon^2 \hat{K}_h^4 + c^4},$$

$\mathfrak{J}_{IPR}(h, c, \epsilon)$ is given by (3.5) with explicit ϵ -dependence due to $K_\tau = \sqrt{\epsilon}$, and

$$(4.17) \quad \mathfrak{J}_{SERCA}^+(c) = \hat{V}_s \left(\frac{c^2}{K_s^2 + c^2} \right), \quad \mathfrak{J}_{SERCA}^-(c) = \hat{K} \gamma^2 \hat{V}_s \left(\frac{(c_t - c)^2}{K_s^2 + c^2} \right).$$

By considering $\epsilon \ll 1$, system (4.15) can be written as the series expansion

$$(4.18) \quad \begin{aligned} \begin{pmatrix} h' \\ c' \end{pmatrix} &= \begin{pmatrix} -\hat{\tau}_{\max}^{-1} \\ \mathfrak{J}_{IPR}^{(0)}(h, c) \end{pmatrix} c^4 h + \epsilon \begin{pmatrix} 0 \\ -\mathfrak{J}_{SERCA}^+(c) \end{pmatrix} \\ &+ \epsilon^2 \begin{pmatrix} \hat{\tau}_{\max}^{-1} (\hat{K}_h^4 - h) \\ \mathfrak{J}_{IPR}^{(1)}(h, c) c^8 h + \mathfrak{J}_{SERCA}^-(c) \end{pmatrix} + \epsilon^4 \begin{pmatrix} R_{h_\infty}(c, \epsilon) \\ R_{IPR}(h, c, \epsilon) \end{pmatrix}, \end{aligned}$$

with IPR terms

$$\mathfrak{J}_{IPR}^{(k)}(h, c) := \left(\frac{1}{c^{4(k+1)} h} \right) k_{IPR} P_O^{(k)}(h, c, 0) (\gamma c_t - (1 + \gamma) c), \quad k = 0, 1,$$

where

$$(4.19) \quad \begin{aligned} P_O^{(0)}(h, c) &= \frac{p^2 c^4 h}{p^2 (1 + k_\beta) c^4 h + k_\beta K_p^2 (K_c^4 + c^4)}, \\ P_O^{(1)}(h, c) &= \frac{k_\beta K_p^2 p^2 c^4 h}{(c^4 h (k_\beta + 1) p^2 + k_\beta K_p^2 (c^4 + K_c^4))^2}. \end{aligned}$$

The remainder terms $R_{h_\infty}(c, \epsilon)$ and $R_{IPR}(h, c, \epsilon)$ are $O(1)$ as $\epsilon \rightarrow 0$.

Proof. System (4.15) is obtained from system (4.2) after making the substitutions in (4.6) and (4.12), applying the common scaling (4.13), and dividing both sides of the equation for h' by $\tau_h(c)$.

The expansion in (4.18) follows after significant but standard algebraic manipulations and Taylor expansion in ϵ . \square

Systems (4.15) and (4.18) will be considered in detail in the following section, where we present a GSPT analysis of the dynamics for $0 < \epsilon \ll 1$. Since only these systems will be considered in the remainder of the manuscript, we will drop the hat notation on rescaled parameters, for the sake of readability. Final system parameters are given in Table 3.

5. Multiple time-scale analysis. Having derived a singular perturbation problem via ‘pre-processing’ steps (I)-(III) in Section 4, it remains to carry out step (IV), i.e., a singular perturbation analysis of system (4.18). This will allow us to prove existence and uniqueness of stable three-time-scale relaxation oscillations in the singularly perturbed formulation (4.18).

It is worth noting (see also Section 5.3 and Remark 5.10 below), that a simple existence result for the limit cycle can also be derived using standard phase plane arguments and the Poincaré-Bendixson theorem. While such an approach has the advantage of simplicity, singular perturbation analyses are typically better suited to uncovering detailed information about the geometric and multiple time-scale structure of the oscillations. Our analysis allows for a clear identification of the dominant physiological processes controlling each phase of the limit cycle. There are also methodological motivations for the use of singular perturbation arguments. In particular, the methods developed and applied herein can be readily adapted and applied to multiple time-scale problems in higher dimensions.

System (4.18) is not in the standard form for slow-fast systems, but can be written in the general form

$$(5.1) \quad \begin{pmatrix} h' \\ c' \end{pmatrix} = g(h, c) + \sum_{j \geq 1} \epsilon^j W_j(z) = N(h, c)f(h, c) + \epsilon G(h, c, \epsilon), \quad 0 < \epsilon \ll 1,$$

where $g(h, c) := N(h, c)f(h, c)$, with

$$N(h, c) = \begin{pmatrix} -\tau_{\max}^{-1} \\ \mathfrak{J}_{\text{IPR}}^{(0)}(h, c) \end{pmatrix}, \quad f(h, c) = c^4 h,$$

and $G(h, c, \epsilon) := \sum_{j \geq 1} \epsilon^j W_j(z)$ is given by

$$G(h, c, \epsilon) = \begin{pmatrix} 0 \\ -\mathfrak{J}_{\text{SERCA}}^+(c) \end{pmatrix} + \epsilon \begin{pmatrix} \tau_{\max}^{-1}(K_h^4 - h) \\ \mathfrak{J}_{\text{IPR}}^{(1)}(h, c)c^8 h + \mathfrak{J}_{\text{SERCA}}^-(c) \end{pmatrix} + \epsilon^3 \begin{pmatrix} R_{h_\infty}(c, \epsilon) \\ R_{\text{IPR}}(h, c, \epsilon) \end{pmatrix}.$$

Singular perturbation problems in the general (non-standard) form (5.1) frequently arise in applications, and have been studied using a combination of GSPT and blow-up techniques in, e.g., [19, 15, 21, 30, 33, 32]. For a formal introduction to the use of GSPT in analysing problems in the general form (5.1), we refer the reader to [17] for the planar case, and to [13, 47] for the general (dimension $n \geq 2$) case. See also [25, 32, 31] for applications to systems with $m > 2$ time-scales.

It is important to realise that the presence of switching in system (5.1) leads to distinct limiting systems depending on calcium concentration c . Specifically, for small c , if we write $c = \sqrt{\epsilon}C$ with $C = O(1)$, we have

$$\lim_{\epsilon \rightarrow 0} \mathfrak{h}_\infty(\sqrt{\epsilon}C, \epsilon) = \frac{K_h^4}{K_h^4 + C^4},$$

while for $c = O(1)$, the limit $\lim_{\epsilon \rightarrow 0} \mathfrak{h}_\infty(c, \epsilon)$ is given by the second expression in (4.10). Such observations lead to the identification of two non-overlapping regimes:

- (R1) $c \in \mathcal{I}_1 = [a, b]$ for some fixed a and b with $0 < a < b$;
- (R2) $c \in \mathcal{I}_2 = [0, \sqrt{\epsilon}\nu]$ for some fixed $\nu > 0$.

For sufficiently small $\epsilon \ll 1$, $c = O(1)$ in (R1) and $c = O(\sqrt{\epsilon})$ in (R2). Singular limit analyses in regimes (R1) and (R2) will provide sufficient information for the statement of our main result in Section 5.3. The observed dynamics and corresponding analysis is qualitatively similar, but not identical, to the autocatalator model considered in [19]. Similar systems have also been studied in the (R2) regime only in [28].

Remark 5.1. The right-hand-side in (5.1) is C^∞ for each fixed $0 < \epsilon \ll 1$, but only C^r (for some $r \geq 0$) in the limit $\epsilon \rightarrow 0$ due to a jump discontinuity in the switch terms. In general, the order r is important since it imposes analytical and methodological constraints, particularly if $r = 0$. In the case of system (4.18), we have $r = 2$ because of the term $\mathfrak{h}_\infty(c, \epsilon)\epsilon^2$, since $\mathfrak{h}_\infty(c, \epsilon)$ is discontinuous at $c = \epsilon = 0$. The case $r = 0$ can arise in applications [24], in which case, the resulting perturbation problem can be understood as a smooth perturbation of a piecewise-smooth dynamical system.

5.1. Multiple time-scale analysis in regime (R1). We first consider the dynamics in regime (R1). Setting $\epsilon = 0$ in (5.1) gives the *layer problem*,

$$(5.2) \quad \begin{pmatrix} h' \\ c' \end{pmatrix} = N(h, c)f(h, c) = \begin{pmatrix} -\tau_{\max}^{-1} \\ \mathfrak{J}_{\text{IPR}}^{(0)}(h, c) \end{pmatrix} c^4 h,$$

which has two lines of equilibria, or *critical manifolds*,

$$(5.3) \quad S_c = \{(0, c) : c \geq 0\}, \quad S_h = \{(h, 0) : h \geq 0\}.$$

Remark 5.2. In contrast to standard form slow-fast systems (see, e.g., [29]), there is no globally defined slow variable in system (4.18). Hence the layer problem (5.2) is *not* a bifurcation problem in either h or c .

Evaluating the Jacobian at any given $p \in S_c$ or S_h yields a trivial eigenvalue $\lambda_0 \equiv 0$, whose corresponding eigenvector spans the corresponding tangent space at p . Direct calculations provide the associated non-trivial eigenvalue $\lambda_c(c)$ (resp. $\lambda_h(h)$) of S_c (resp. S_h), given by the Lie derivative expressions

$$(5.4) \quad \lambda_c(c) = \langle \nabla f, N \rangle|_{S_c} = -\tau_{\max}^{-1} c^4 \leq 0, \quad \lambda_h(h) = \langle \nabla f, N \rangle|_{S_h} \equiv 0,$$

see also [17, eqn. (3.7)]. Hence, the manifold S_c is normally hyperbolic and attracting for all $c > 0$, and degenerate at $(0, 0)$. The manifold S_h is degenerate.

Fast fibers constitute non-trivial heteroclinic connections between S_h and S_c in the layer problem (5.2). In particular, they obey the equation

$$(5.5) \quad \frac{dc}{dh} = -\tau_{\max} \mathfrak{J}_{\text{IPR}}^{(0)}(h, c) \begin{cases} < 0 & \text{if } c < \left(\frac{\gamma}{1+\gamma}\right) c_t, \\ = 0 & \text{if } c = \left(\frac{\gamma}{1+\gamma}\right) c_t, \\ > 0 & \text{if } c > \left(\frac{\gamma}{1+\gamma}\right) c_t, \end{cases}$$

see Figure 5.

Remark 5.3. The expressions in (5.5) are not on their own sufficient to prove that orbits of the layer problem connect points on S_h and S_c . A proof of this property follows from Lemma A.4 in Appendix A, and is omitted here for expository reasons.

Next, we consider (5.1) on the slow time-scale $\tau = \epsilon t$, i.e.,

$$(5.6) \quad \epsilon \begin{pmatrix} \dot{h} \\ \dot{c} \end{pmatrix} = N(h, c)f(h, c) + \epsilon G(h, c, \epsilon), \quad 0 < \epsilon \ll 1.$$

The following result (see [17]) considers the limit $\epsilon \rightarrow 0$ of (5.6), called the *reduced problem*, which describes the leading order slow flow on S_c :

LEMMA 5.4. *Given a planar singular perturbation problem in the general form (5.1), with critical manifold S , and normally hyperbolic submanifold $S_n \subset S$. Then the reduced problem on S_n is given by*

$$(5.7) \quad \begin{pmatrix} \dot{h} \\ \dot{c} \end{pmatrix} = \left[\frac{\det(N|G)}{\langle \nabla f, N \rangle} \begin{pmatrix} -D_c f \\ D_h f \end{pmatrix} \right] \Big|_{S_n},$$

where the $(\dot{\cdot})$ notation denotes differentiation with respect to slow time τ , and the determinant $\det(N|G)$ is taken with respect to the matrix with columns $N(h, c)$ and $G(h, c, 0)$.

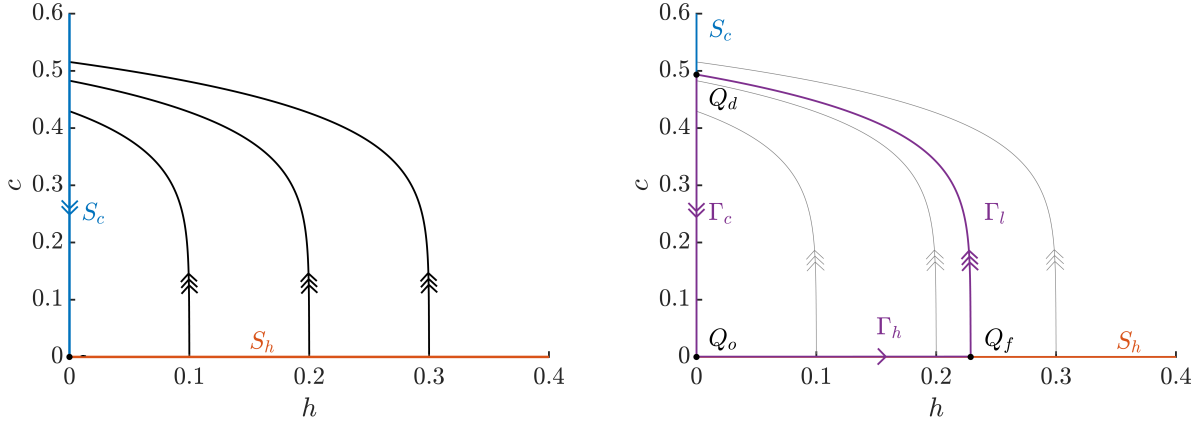


Fig. 5: Singular limit dynamics. (Left) The (nonlinear) fast connection from S_h to S_c is determined by the layer problem (5.2) and the flow on S_c is given by the reduced problem (5.8). The manifold S_h is degenerate. (Right) The singular orbit $\Gamma = \Gamma_h \cup \Gamma_c \cup \Gamma_l$. Note, the flow indicated on S_h is not formally defined, and included for illustrative purposes only; it represents the rightward motion along $\mathcal{S}_{a,\delta}$ in Figure 6, and helps to illustrate the three-time-scale structure of the oscillations.

Proof. The expression in (5.7) is obtained by projecting the leading order perturbation vector $G(h, c, 0)$ at each point $p \in S_c \setminus \{(0, 0)\}$ onto its component in the corresponding tangent space $T_p S_c$; see [17, Proposition 3.4]. See also [10, 13, 47] for similar methods applicable in the case that the dimension n is greater than two. \square

We obtain an expression for the reduced problem on $S_c \setminus \{0, 0\}$ directly via equation (5.7), which gives

$$(5.8) \quad \begin{pmatrix} \dot{h} \\ \dot{c} \end{pmatrix} = \begin{pmatrix} 0 \\ -\mathfrak{J}_{\text{SERCA}}^+(c) \end{pmatrix}.$$

In particular, $-\mathfrak{J}_{\text{SERCA}}^+(c) < 0$ for all $c > 0$ and $-\mathfrak{J}_{\text{SERCA}}^+(0) = 0$; the reduced flow on S_c is toward the origin. The origin itself can be considered as a non-hyperbolic equilibrium for the reduced problem extended to all of S_c ; see Figure 5.

The preceding analysis for both layer and reduced problems implies the following result for $0 < \epsilon \ll 1$, which follows by classical results due to Fenichel [10].

LEMMA 5.5. *There exists an $\epsilon_0 > 0$ such that for all $\epsilon \in (0, \epsilon_0]$, compact submanifolds of S_c perturb to $O(\epsilon)$ -close locally invariant one-dimensional slow manifolds*

$$S_{c,\epsilon} = \{(\tilde{v}(c, \epsilon), c) : c \in [c_-, c_+]\},$$

where $\tilde{v}(c, \epsilon) = O(\epsilon)$, and c_{\pm} are positive constants satisfying $c_+ > c_- > 0$. The leading order flow on each $S_{c,\epsilon}$ is governed by the reduced problem (5.8).

It remains to understand the dynamics near the degenerate line S_h . For this we must look in regime (R2).

5.2. Multiple time-scale analysis in regime (R2). We now consider the dynamics in regime (R2), where $c = O(\sqrt{\epsilon})$. We work in the rescaled coordinates $(h, c) = (h, \sqrt{\epsilon}C)$ and define

$$\delta := \sqrt{\epsilon}$$

for simplicity, i.e., in order to avoid fractional exponents. Rewriting system (5.1) in the new rescaled coordinates on an ‘intermediate-slow’ time-scale $t_1 = \epsilon^{3/2}t = \delta^3t$ yields

$$(5.9) \quad \begin{pmatrix} h' \\ C' \end{pmatrix} = \tilde{N}(h, C)\tilde{f}_0(h, C) + \delta\tilde{G}(h, C, \delta), \quad 0 < \delta \ll 1,$$

where

$$(5.10) \quad \tilde{N}(h, C) = \begin{pmatrix} 0 \\ 1 \end{pmatrix}, \quad \tilde{f}_0(h, C) = A_{\text{IPR}}\gamma c_t C^4 h - A_{\text{SERCA}}(C^2 - K\gamma^2 c_t^2),$$

and

$$(5.11) \quad \tilde{G}(h, C, \delta) = \begin{pmatrix} \tilde{g}(h, C) \\ \tilde{f}_{\text{rem}}(C, h, \delta) \end{pmatrix} = \begin{pmatrix} -\tau_h(C)^{-1}(h - h_\infty(C)) \\ -(A_{\text{IPR}}(1 + \gamma)C^4 h + 2A_{\text{SERCA}}c_t)C + O(\delta) \end{pmatrix}.$$

In the above we defined

$$A_{\text{IPR}} = \left(\frac{k_{\text{IPR}}p^2}{k_\beta K_c^4 K_p^2} \right), \quad A_{\text{SERCA}} = \frac{V_s}{K_s^2},$$

and permitted a slight abuse of notation by letting the prime ($'$) denote differentiation with respect to the new intermediate-slow time t_1 . In writing (5.11), we also appeal to the fact that $\mathfrak{h}_\infty(\delta C, \delta^2) = h_\infty(C)$. Finally, note that $\tilde{f}_0(h, C)$ is just the leading order term in an expansion in δ , and that in this regime, IPR and SERCA processes compete at leading order.

Remark 5.6. System (5.9) is in the so-called standard form for slow-fast systems. We present it here in the general form (5.1), and proceed via the same (more general) approach adopted in Section 5.1. Our reasons for doing so are three-fold: (i) consistency with earlier sections is maintained; (ii) there are no additional technical difficulties, and (iii) this approach illustrates the relationship between the theory developed for standard form problems and its non-standard form generalisation.

Setting $\delta = 0$ in (5.9) yields the layer problem

$$(5.12) \quad \begin{pmatrix} h' \\ C' \end{pmatrix} = \tilde{N}\tilde{f}_0(h, C) = \begin{pmatrix} 0 \\ 1 \end{pmatrix} (A_{\text{IPR}}\gamma c_t C^4 h - A_{\text{SERCA}}(C^2 - K\gamma^2 c_t^2)),$$

which has critical manifold

$$(5.13) \quad \mathcal{S} = \{(\zeta(C), C) : C \geq 0\}, \quad \zeta(C) = \frac{A_{\text{SERCA}}}{A_{\text{IPR}}\gamma c_t C^4} (C^2 - K\gamma^2 c_t^2),$$

see Figure 6. The non-trivial eigenvalue along \mathcal{S} is given by the Lie derivative expression

$$(5.14) \quad \lambda_{\mathcal{S}}(C) = \langle \nabla f, N \rangle|_{\mathcal{S}} = D_C \tilde{f}_0(\zeta(C), C) = \frac{2A_{\text{SERCA}}}{C} (C^2 - 2K\gamma^2 c_t^2).$$

The manifold \mathcal{S} has a fold point at

$$(5.15) \quad F = (\zeta(C_F), C_F) = \left(\frac{A_{\text{SERCA}}}{4K\gamma^3 c_t^3 A_{\text{IPR}}}, \sqrt{2K}\gamma c_t \right),$$

where $\lambda_{\mathcal{S}}(C_F) = 0$ and the following nondegeneracy conditions are satisfied:

$$(5.16) \quad D_C^2 \tilde{f}_0(\zeta(C_F), C_F) = 4A_{\text{SERCA}} > 0, \quad D_h \tilde{f}_0(\zeta(C_F), C_F) = 4A_{\text{IPR}}K^2\gamma^5 c_t^5 > 0.$$

The first inequality in (5.16) implies that $\mathcal{S} = \mathcal{S}_a \cup \{F\} \cup \mathcal{S}_r$, where

$$\mathcal{S}_a = \{(\zeta(C), C) : 0 < C < C_F\}, \quad \mathcal{S}_r = \{(\zeta(C), C) : C > C_F\},$$

and \mathcal{S}_a (resp. \mathcal{S}_r) is normally hyperbolic and attracting (resp. repelling), as sketched in Figure 6.

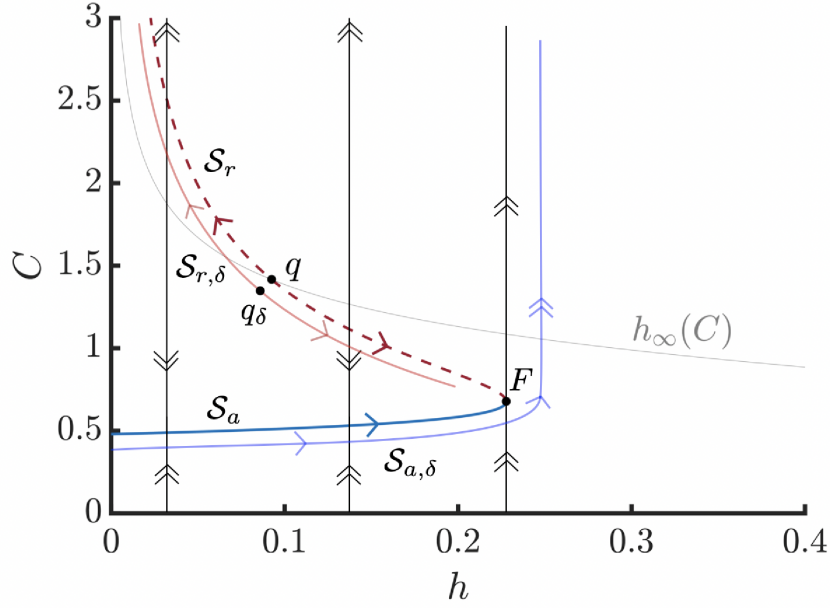


Fig. 6: Sketch of the dynamics in regime (R2). The critical manifold $\mathcal{S} = \mathcal{S}_a \cup \{F\} \cup \mathcal{S}_r$ is shown with \mathcal{S}_a in blue and \mathcal{S}_r in dashed red. The fold point F , equilibrium q and h -nullcline (in grey) are also indicated. Perturbed slow manifolds $\mathcal{S}_{a,\delta}$ and $\mathcal{S}_{r,\delta}$ are shown in shaded blue and red respectively, with the attracting slow manifold $\mathcal{S}_{a,\delta}$ extending through the neighbourhood of the fold point F as described by Lemma 5.8.

Now consider the reduced problem on the manifold \mathcal{S} , which describes the leading order dynamics on the infra-slow time-scale $\tau_1 = \delta t_1 = \epsilon^2 t$. As in Section 5.1, we use the formula (5.7) to derive the reduced problem,

$$(5.17) \quad \begin{pmatrix} \dot{h} \\ \dot{C} \end{pmatrix} = \left[\frac{\det(\tilde{N}|\tilde{G})}{\langle \nabla \tilde{f}_0, \tilde{N} \rangle} \begin{pmatrix} -D_c \tilde{f}_0 \\ D_h \tilde{f}_0 \end{pmatrix} \right] \Big|_{\mathcal{S}} = \begin{pmatrix} 1 \\ -\frac{D_h \tilde{f}_0(\zeta(C), C)}{\lambda_{\mathcal{S}}(C)} \end{pmatrix} \tilde{g}(\zeta(C), C),$$

where by another (slight) abuse of notation, (\cdot) refers to differentiation with respect to the infra-slow time-scale τ_1 . Explicitly, we obtain the system

$$(5.18) \quad \begin{pmatrix} \dot{h} \\ \dot{C} \end{pmatrix} = \begin{pmatrix} -\tau_h(C)^{-1} \\ \frac{A_{\text{IPR}} \gamma c_t C^5}{2A_{\text{SERCA}} \tau_h(C) (C^2 - 2K\gamma^2 c_t^2)} \end{pmatrix} (\zeta(C) - h_{\infty}(C)).$$

Remark 5.7. In total we have identified *four* distinct time-scales in system (5.1) that are involved in our analysis (fast, slow, intermediate-slow, infra-slow):

$$t, \quad \tau = \epsilon t, \quad t_1 = \delta^3 t = \epsilon^{3/2} t, \quad \tau_1 = \delta t_1 = \epsilon^2 t.$$

System (5.18) can have up to three equilibria $(\varphi(C_*), C_*) \in \mathcal{S}$ in the physiological domain $h, C \geq 0$. Their locations can be determined by solving the equation

$$\zeta(C) = h_{\infty}(C),$$

which reduces to the problem of identifying positive, real-valued roots of the cubic equation

$$(5.19) \quad P(m) = \alpha_3 m^3 + \alpha_2 m^2 + \alpha_1 m + \alpha_0 = 0,$$

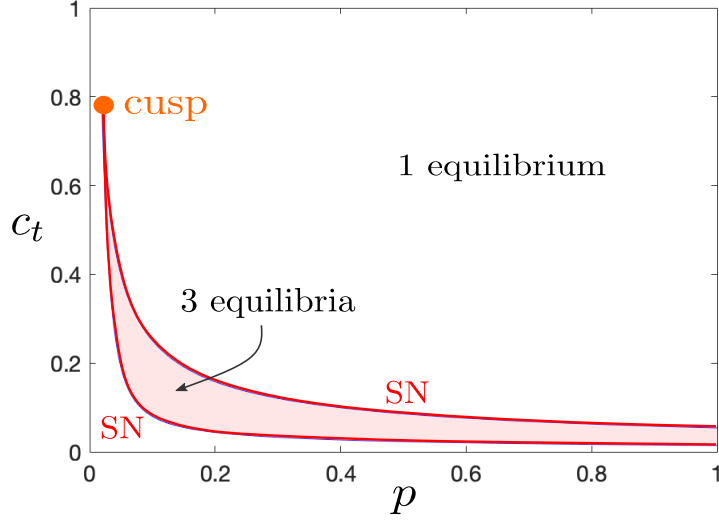


Fig. 7: Number of equilibria in (p, c_t) -parameter space. The region with three equilibria is bounded by two codimension-one saddle-node branches emanating from a codimension-two cusp point at $(p, c_t) \sim (0.02, 0.8)$; outside this region there exists a unique equilibrium. Parameter values are as in Table 3.

obtained after setting $m = C^2$. The coefficients α_i , $i = 0, 1, 2, 3$ are given by

$$(5.20) \quad \begin{aligned} \alpha_3 &= \frac{A_{\text{SERCA}}}{\gamma c_t A_{\text{IPR}}}, & \alpha_2 &= -K_h^4 - \frac{A_{\text{SERCA}}}{A_{\text{IPR}}} K \gamma c_t, \\ \alpha_1 &= \frac{K_h^4 A_{\text{SERCA}}}{\gamma c_t A_{\text{IPR}}}, & \alpha_0 &= -\frac{K K_h^4 \gamma c_t A_{\text{SERCA}}}{A_{\text{IPR}}}. \end{aligned}$$

Note that the number of real-valued roots for equation (5.19) depends on the system parameters p and c_t ; see Figure 7, which identifies a cusp structure in (p, c_t) -space.

Of course, the location and stability properties of the corresponding equilibria for system (5.17) will also depend on these parameters. We are interested here in the case in which system (5.17) has a unique, unstable equilibrium $q \in \mathcal{S}_r$.

Assumption 5.1. The parameters p , c_t are chosen so that the cubic polynomial $P(m)$ in (5.19) has a unique positive real-valued root, such that system (5.17) has a unique equilibrium $q = (\varphi(C_*), C_*) \in \mathcal{S}$. Moreover, we require that

$$(5.21) \quad \frac{2A_{\text{IPR}}K_h^4\gamma c_t}{A_{\text{SERCA}}} > \frac{1}{C_*^8} (K_h^4 + C_*^4) (C_*^2 - C_F^2) > 0,$$

implying that q is unstable on \mathcal{S}_r .

The rightmost inequality in equation (5.21) implies that $C_* > C_F$, so that $q \in \mathcal{S}_r$. The leftmost inequality ensures that $D_C \dot{C}|_{C=C_*} > 0$, so that q is unstable as an equilibrium on \mathcal{S} . Note that Assumption 5.1 is satisfied for the parameter values in Table 3, for which we have a unique equilibrium $q \approx (0.074, 1.48) \in \mathcal{S}_r$ satisfying $C_* \approx 1.48 > C_F \approx 0.68$ and

$$\frac{2A_{\text{IPR}}K_h^4\gamma c_t}{A_{\text{SERCA}}} \approx 17.01 > \frac{1}{C_*^8} (K_h^4 + C_*^4) (C_*^2 - C_F^2) \approx 0.391 > 0.$$

Assumption 5.1 also implies that the regularity conditions

$$(5.22) \quad \tilde{g}(\zeta(C_F), C_F) \neq 0, \quad D_C \tilde{g}(\zeta(C_F), C_F) \neq 0,$$

at the fold point F are fulfilled.

Note that the reduced problem (5.17) is not defined at F , since the flow undergoes a finite time blow-up (solutions reach F in finite time). The conditions in (5.22) imply that the reduced flow is oriented locally toward F , classifying the regular fold as a *regular jump point* [29], where there is a transition from slow to fast.

The dynamics for $0 < \delta \ll 1$ in compact subdomains in regime (R2) are well-described by existing theory, and summarised in the following result.

LEMMA 5.8. *Given system (5.9) and Assumption 5.1, there exists $\delta_0 > 0$ such that for all $\delta \in (0, \delta_0]$ compact submanifolds of \mathcal{S}_a and \mathcal{S}_r perturb to $O(\delta)$ -close locally invariant slow manifolds of the form*

$$\mathcal{S}_{a,\delta} = \{(\zeta(C) + O(\delta), C) : C \in [C_-, C_+]\}, \quad \mathcal{S}_{r,\delta} = \{(\zeta(C) + O(\delta), C) : C \in [C_l, C_r]\},$$

respectively, where C_\pm and $C_{l,r}$ are any positive constants satisfying $0 < C_- < C_+ < C_F$ and $C_F < C_l < C_r < \infty$. The leading order flow on $\mathcal{S}_{a/r,\delta}$ is given by the reduced flow on $\mathcal{S}_{a/r}$, and the reduced flow equilibrium $q \in \mathcal{S}_r$ perturbs to a nearby equilibrium $q_\delta \in \mathcal{S}_{r,\delta}$ of unstable node type.

The attracting slow manifolds $\mathcal{S}_{a,\delta}$ extend through a neighbourhood of the regular jump point, exiting along the fast flow which is $O(\delta^{2/3})$ -close to the fast fiber $\{(\zeta(C_F), C) : C > C_F\}$; see Figure 6.

Proof. The dynamics bounded away from a neighbourhood of F , including the persistence of the unstable node q_δ , is described by Fenichel theory [10]. The dynamics near F is described by [26, Theorem 2.1]. \square

It follows that trajectories are either repelled to infinity or exponentially attracted to slow manifolds $\mathcal{S}_{a,\delta}$, after which they follow the slow flow up to the neighbourhood of the regular jump point F , before leaving via the fast flow. Once on the fast flow, the global separation of slow and fast variables in regime (R2) prohibits the existence of a return mechanism on any compact domain. Limit cycles for $0 < \delta \ll 1$ must traverse both regimes (R1) and (R2).

5.3. Existence and uniqueness of the relaxation oscillations. We now use the results of the preceding sections in order to state an existence and uniqueness result for relaxation oscillations in system (5.1), in the (p, c_t) -parameter region specified by Assumption 5.1.

We consider system (5.1) in regime (R1), for which the fold point F identified in regime (R2) ‘collapses’ onto the point $Q_f = (h_F, 0) = (\zeta(C_F), 0) \in S_h$. Having identified this point, we can construct the singular orbit

$$\Gamma = \Gamma_c \cup \Gamma_h \cup \Gamma_l,$$

where

$$\Gamma_h = \{(h, 0) : h \in [0, h_F]\}, \quad \Gamma_c = \{(0, c) : c \in [0, c_d]\},$$

and Γ_l is the (unique) heteroclinic orbit of the layer problem (5.2) connecting Q_f to the ‘drop point’ $Q_d = (0, c_d) \in S_c$; see Figure 5 (Right). It should be noted that because of curvature in the layer flow, existence of a drop point $Q_d \in S_c$ must be shown explicitly (recall Remark 5.3).

THEOREM 5.9. *Consider system (5.1) with (p, c_t) fixed within the region specified by Assumption 5.1. There exists an $\epsilon_0 > 0$ such that for all $\epsilon \in (0, \epsilon_0)$, there exists a relaxation cycle Γ_ϵ which is $O(\epsilon^{1/3})$ -close to the singular orbit Γ in the Hausdorff distance as $\epsilon \rightarrow 0$. The relaxation cycle Γ_ϵ is exponentially attracting, with Floquet exponent bounded above by $-\kappa/\epsilon^2$ for some constant $\kappa > 0$. Moreover, for any fixed $M > 0$ such that Γ_ϵ is contained within the ball $B(0, M)$, choosing $\epsilon_0 > 0$ sufficiently small guarantees that Γ_ϵ is the only limit cycle in $B(0, M)$.*

Theorem 5.9 states existence and uniqueness for the relaxation cycles observed in Figure 1. Note that the $O(\delta)$ time-scale separation in regime (R2) (as opposed to the $O(\epsilon)$ time-scale separation in regime (R1)) leads to a relaxation cycle Γ_ϵ which is $O(\epsilon^{1/3})$ from Γ , in contrast to the usual $O(\epsilon^{2/3})$ separation associated with two time-scale relaxation oscillations; see, e.g., [27, 29]. This is a consequence of the $O(\delta^{2/3}) = O(\epsilon^{1/3})$ separation near the fold in the regime (R2), as described in Lemma 5.8. The bound $-\kappa/\epsilon^2$ on the Floquet exponent also differs from the usual $-\kappa/\epsilon$ bound. This is a consequence of the total time spent in the vicinity of the attracting slow manifold $\mathcal{S}_{a,\delta}$, which is $O(1)$ on the infra-slow time-scale $\tau_1 = \epsilon^2 t$.

The proof of Theorem 5.9 utilises the so-called *blow-up method* [8] in the formulation of [26, 27]. Due to the length of the proof and the conceptual similarities with the analysis undertaken for the autocatalator problem in [19], this is deferred to Appendix A. The main task is to resolve the degeneracy associated with the non-hyperbolic line S_h and, in particular, the point $Q_o = (0, 0)$. This can be achieved in a two-step process, by means of a cylindrical blow-up along S_h , and a second (successive) spherical blow-up necessary to resolve a persistent degeneracy stemming from the point Q_o . We refer the interested reader to Figures 9 and 10 in particular, which illustrate the main dynamical features after blow-up and further illustrate the similarity with the autocatalator model presented in [19].

Remark 5.10. As noted in the introductory discussion of this section, one can also prove the existence of a limit cycle in system (5.1) by an application of the Poincaré-Bendixson theorem, i.e., without recourse to blow-up techniques. However, very little dynamical insight relating to the geometric structure of the oscillations is obtained via such an argument. Importantly, the role of different flux terms in producing different phases of the oscillations is revealed via GSPT analysis, insofar as each segment of the singular relaxation cycle in Figure 5 (or, more precisely, Figure 9) perturbs to a phase of the oscillation that is dominated by one or more flux terms. Specifically, the fast transition bounded away from the h and c axes is governed by the layer problem (5.2). Here, the flux terms $h/\tau_h(c)$ and $J_{\text{IPR}}(h, c)$ are active, and dominate the dynamics. The phase of the oscillations corresponding to vertical flow down the c -axis is governed by the reduced problem (5.8) where $J_{\text{SERCA}}^+(c)$ is active, and the phase of the oscillations corresponding to flow along the h -axis is governed by the reduced problem (5.18), where all five flux terms play a role in determining the dynamics. The characteristic time-scale associated with each phase of the oscillation is also revealed via the GSPT approach; see again Remark 5.7. Finally we note that approaches based on GSPT and blow-up techniques can be lifted to higher dimensions, and therefore provide a natural geometric approach for the analysis of ODE models characterised by multiple time-scales and/or switching more generally.

Our analysis also allows for a leading order approximation of the oscillation period \mathcal{T} as a function of the model parameter τ_{max} , as in the following Proposition. Our results are consistent with numerical findings in [45], where τ_{max} is shown to play an important role in determining the period of oscillations in the three-dimensional open-cell model (3.1).

PROPOSITION 5.11. *Consider system (5.1) with (p, c_t) fixed within the region specified by Assumption 5.1. Then there exists an $\epsilon_0 > 0$ such that for all $\epsilon \in (0, \epsilon_0)$, the leading order approximation for the period \mathcal{T} of the relaxation cycle Γ_ϵ is linear in τ_{max} . More precisely, written in terms of the fast time-scale t of system (5.1) we have*

$$\mathcal{T} \sim \epsilon^{-2} \tau_{\text{max}} v(p, c_t) \quad \text{as} \quad \epsilon \rightarrow 0,$$

where $v(p, c_t)$ is smooth, positive and bounded on the relevant domain.

Proof. Assuming Theorem 5.9, the leading order approximation for the period \mathcal{T} as $\epsilon \rightarrow 0$ is determined by the total time spent in the vicinity of the attracting infra-slow manifold \mathcal{S}_a . This can be approximated using the expression for the corresponding reduced flow given in (5.17) which evolves on the infra-slow time-scale $\tau_1 = \epsilon^2 t$. Let $C(\tau_1)$ denote a solution for (5.17) such that $\zeta(C(0)) = 0$ and $C(\tau_1^0) = C_F$ for some $\tau_1^0 = \epsilon^2 t_0 > 0$. This yields $C(0) = \sqrt{K} \gamma_{c_t}$ and $C(\tau_1^0) = \sqrt{2K} \gamma_{c_t}$, and hence

$$(5.23) \quad \epsilon^2 \mathcal{T} \sim \int_0^{\tau_1^0} d\tau_1 = \int_{\sqrt{K} \gamma_{c_t}}^{\sqrt{2K} \gamma_{c_t}} \frac{1}{\dot{C}} dC,$$

where ϵ^2 appears in the left-hand-side since we aim to approximate the period \mathcal{T} on the fast time-scale $t = \epsilon^{-2} \tau_1$ of system (5.1).

Using (5.17), the integrand can be written as $1/\dot{C} = \tau_{\text{max}} V(C; p, c_t)$, where the function $V(C; p, c_t)$ is smooth with respect to C, c_t, p , and independent of τ_{max} . By Assumption 5.1 we have that $\dot{C} > 0$, and hence $V(C; p, c_t) > 0$ on \mathcal{S}_a . Thus, as $\epsilon \rightarrow 0$,

$$\mathcal{T} \sim \epsilon^{-2} \tau_{\text{max}} \int_{\sqrt{K} \gamma_{c_t}}^{\sqrt{2K} \gamma_{c_t}} V(C; p; c_t) dC = \epsilon^{-2} \tau_{\text{max}} v(p, c_t),$$

where $v(p, c_t)$ is some smooth, positive and bounded function. □

Remark 5.12. Figure 1 shows relaxation oscillations with an approximate period $\mathcal{T} \approx 2 \times 10^4$, which compares well to the order estimate $\epsilon^{-2}\tau_{\max} \approx 5 \times 10^4$ derived above and evaluated using the parameter values given in Table 3.

Finally, we refer the interested reader to Appendix B for additional results pertaining to the onset of the relaxation oscillations under parameter variation. Here we provide numerical evidence for the explosive onset of relaxation oscillations under variation of the total calcium c_t . Such findings are particularly relevant for future analyses of the three-dimensional open cell model (3.2), where c_t is a slow variable. We also provide an analytical result describing the gradual (i.e., non-explosive) onset of oscillations under variation of the parameter τ_{\max} , confirming previous observations in [45] on the role of τ_{\max} as an important parameter for controlling the existence and period of oscillations in models for intracellular calcium dynamics.

6. Discussion and Conclusion. Time-scale separation and switching are ubiquitous in models of biological and physiological phenomena, but literature on the analysis of such systems, particularly via methods of geometric singular perturbation theory, is relatively sparse. There are a number of reasons for this. The first significant obstacle to analysis of such models concerns the identification of suitable perturbation parameters, since these are frequently not explicit in a model. In the case that one or more perturbation parameters can be identified, a second obstacle arises if there is more than one, namely, the question of how to relate or order perturbation parameters in such a way that the resulting singular perturbation problem is both tractable and reliable as an approximation of the original model. Finally, there are obstacles relating to the mathematical analysis of the resulting singular perturbation problem; singular perturbation problems derived from ODE models for chemical, biological and physiological phenomena are frequently characterised by non-standard time-scale separations, more than two time-scales, and loss of smoothness in the singular limit due to switching, all of which can complicate the analysis.

In this work, we have outlined a heuristic procedure for the formulation as singular perturbation problems of ODE models characterised by multi-scale dynamics and/or switching. The procedure was sketched in generality in Section 2, and consists of the following steps: (I) non-dimensionalise, (IIa) associate small parameters to maximal process/flux rates, (IIb) associate small parameters to steep switches, (III) relate small parameters, and (IV) analyse the system via perturbation theory.

The procedure was applied in detail in Sections 4-5 to a closed-cell model for intracellular calcium dynamics. Specifically, we identified a total of five small parameters. Three of these small parameters, ϵ_1, ϵ_2 and ϵ_3 , were identified in step (IIa), and correspond to constant pre-factors of particular flux terms (e.g. V_s). The remaining two small parameters, ϵ_4 and ϵ_5 , were identified in step (IIb), and derive from the presence of switching behaviour due to the presence of Hill-type functions with a steep gradient. All five small parameters were related to a single small parameter $\epsilon \ll 1$ via the polynomial scaling (4.13) in step (III), the form of which was based on order of magnitude comparisons. This yielded the singular perturbation problem (4.15) (or equivalently (4.18)) which featured a non-standard time-scale separation; the non-standard time-scale separation stemmed from the presence of small parameters associated with both steps (IIa)-(IIb).

In Section 5 we analysed system (4.18) using the coordinate-independent formulation of GSPT developed in [47]. The non-standard time-scale separation in the model led to distinct scaling regimes (R1) and (R2), with distinct time-scale separations. In the context of biological switching in general, an increasing number of studies show that distinct scaling regimes of this kind are to be expected [19, 21, 24]. These references, along with the current manuscript, also demonstrate the suitability of blow-up methods for combining dynamical information obtained in distinct scaling regimes. We proved existence, uniqueness and stability for the observed three-time-scale relaxation cycles, as described in Theorem 5.9, and provided an estimate for the period of the oscillations in Proposition 5.11. Finally, further results pertaining to the onset of the relaxation oscillations under variation of parameters of interest (p, c_t and τ_{\max}) are described in Appendix B.

We emphasise that there are other, seemingly simpler, methods for proving the existence of relaxation oscillations in the specific calcium dynamics model investigated in this work. In particular, using standard phase plane arguments in combination with the Poincaré-Bendixson theorem might be a natural way to proceed for this two-dimensional model. However, our methods provided additional information on the geometric and time-scale structure of the oscillations which cannot be obtained directly via these other methods. Furthermore, our methods are transferable to higher-dimensional problems (although we acknowledge that their implementation in higher-dimensional models will have challenges.)

There are many directions in which one can take this work. For example, it could be interesting to give a detailed description of the canard and incomplete canard explosions described in Section B.1. The current manuscript also paves the way for rigorous analytical treatment of the higher-dimensional open-cell model from which it is derived. In fact, one could view system (3.3) as a layer problem for the open-cell but ‘almost-closed’ model (3.2) with $|J_{pm}| \ll 1$. In this context, a one-parameter bifurcation analysis of system (4.15) in c_t amounts to an analysis of the layer problem to system (3.2); a three-dimensional system with (at least) four time-scales, due to an additional slow evolution in c_t . The case $|J_{pm}| = O(1)$ corresponding to ‘more open’ cells is also of physiological significance. In both cases, this work provides a solid foundation upon which these significant and highly non-trivial analyses become feasible.

Acknowledgements. The authors would like to thank the associate editor, editor and reviewers of the first submitted version of the manuscript, whose feedback and observations led to significant improvements in the current version.

REFERENCES

- [1] A. ATRI, J. AMUNDSON, D. CLAPHAM, AND J. SNEYD, *A single-pool model for intracellular calcium oscillations and waves in the Xenopus laevis oocyte*, Biophysical Journal, 65 (1993), pp. 1727–1739.
- [2] G. R. BELITSKII, *Functional equations and conjugacy of local diffeomorphisms of a finite smoothness class*, Functional Analysis and Its Applications, 7 (1973), pp. 268–277.
- [3] J. I. BRUCE, T. J. SHUTTLEWORTH, D. R. GIOVANNUCCI, AND D. I. YULE, *Phosphorylation of inositol 1, 4, 5-trisphosphate receptors in parotid acinar cells a mechanism for the synergistic effects of camp on ca2+ signaling*, Journal of Biological Chemistry, 277 (2002), pp. 1340–1348.
- [4] C. A. BUZZI, P. R. DA SILVA, AND M. A. TEIXEIRA, *A singular approach to discontinuous vector fields on the plane*, Journal of Differential Equations, 231 (2006), pp. 633–655.
- [5] P. T. CARDIN AND M. A. TEIXEIRA, *Fenichel theory for multiple time scale singular perturbation problems*, SIAM Journal on Applied Dynamical Systems, 16 (2017), pp. 1425–1452.
- [6] P. DE MAESSCHALCK AND M. WECHSELBERGER, *Neural excitability and singular bifurcations*, The Journal of Mathematical Neuroscience (JMN), 5 (2015), pp. 1–32.
- [7] A. DHOOGHE, W. GOVAERTS, AND Y. A. KUZNETSOV, *MATCONT: a MATLAB package for numerical bifurcation analysis of ODEs*, ACM Transactions on Mathematical Software (TOMS), 29 (2003), pp. 141–164.
- [8] F. DUMORTIER AND R. ROUSSARIE, *Canard cycles and center manifolds*, no. 577 in Memoirs of the American Mathematical Society, American Mathematical Society, 1996.
- [9] G. DUPONT, M. FALCKE, V. KIRK, AND J. SNEYD, *Models of calcium signalling*, vol. 43, Springer, 2016.
- [10] N. FENICHEL, *Geometric singular perturbation theory for ordinary differential equations*, Journal of Differential Equations, 31 (1979), pp. 53–98.
- [11] L. GLASS AND R. EDWARDS, *Hybrid models of genetic networks: mathematical challenges and biological relevance*, Journal of theoretical biology, 458 (2018), pp. 111–118.
- [12] A. GOEKE, C. SCHILLI, S. WALCHER, AND E. ZERZ, *Computing quasi-steady state reductions*, Journal of Mathematical Chemistry, 50 (2012), pp. 1495–1513.
- [13] A. GOEKE AND S. WALCHER, *A constructive approach to quasi-steady state reductions*, Journal of mathematical chemistry, 52 (2014), pp. 2596–2626.
- [14] A. J. HOMBURG AND B. SANDSTEDTE, *Homoclinic and heteroclinic bifurcations in vector fields*, Handbook of Dynamical Systems, 3 (2010), pp. 379–524.
- [15] A. HUBER AND P. SZMOLYAN, *Geometric singular perturbation analysis of the yamada model*, SIAM Journal on Applied Dynamical Systems, 4 (2005), pp. 607–648.
- [16] L. IRONI, L. PANZERI, E. PLAhte, AND V. SIMONCINI, *Dynamics of actively regulated gene networks*, Physica D: Nonlinear Phenomena, 240 (2011), pp. 779–794.
- [17] S. JELBART AND M. WECHSELBERGER, *Two-stroke relaxation oscillators*, Nonlinearity, 33 (2020), p. 2364.
- [18] C. JONES, *Geometric Singular Perturbation Theory, Lecture Notes in Mathematics, Dynamical Systems (Montecatini Terme)*, Springer, Berlin, 1995.
- [19] I. KOSIUK AND P. SZMOLYAN, *Geometric singular perturbation analysis of an autocatalator model*, Discrete and Continuous Dynamical Systems, 2 (2009), pp. 783–806.
- [20] I. KOSIUK AND P. SZMOLYAN, *Scaling in singular perturbation problems: blowing up a relaxation oscillator*, SIAM Journal on Applied Dynamical Systems, 10 (2011), pp. 1307–1343.
- [21] I. KOSIUK AND P. SZMOLYAN, *Geometric analysis of the goldbeter minimal model for the embryonic cell cycle*, Journal of mathematical biology, 72 (2016), pp. 1337–1368.
- [22] K. U. KRISTIANSEN, *The regularized visible fold revisited*, Journal of Nonlinear Science, 30 (2020), pp. 2463–2511, <https://doi.org/10.1007/s00332-020-09627-8>.
- [23] K. U. KRISTIANSEN AND S. J. HOGAN, *Resolution of the piecewise smooth visible-invisible two-fold singularity in R3 using regularization and blowup*, Journal of Nonlinear Science, 29 (2018), pp. 723–787, <https://doi.org/10.1007/s00332-018-9502-x>.
- [24] K. U. KRISTIANSEN AND P. SZMOLYAN, *Relaxation oscillations in substrate-depletion oscillators close to the nonsmooth*

- limit, *Nonlinearity*, 34 (2021), pp. 1030–1083, <https://doi.org/10.1088/1361-6544/abb542>.
- [25] N. KRUFF AND S. WALCHER, *Coordinate-independent singular perturbation reduction for systems with three time scales*, *Mathematical Biosciences and Engineering*, 16 (2019), pp. 5062–5091.
 - [26] M. KRUPA AND P. SZMOLYAN, *Extending geometric singular perturbation theory to nonhyperbolic points—fold and canard points in two dimensions*, *SIAM journal on mathematical analysis*, 33 (2001), pp. 286–314.
 - [27] M. KRUPA AND P. SZMOLYAN, *Relaxation oscillation and canard explosion*, *Journal of Differential Equations*, 174 (2001), pp. 312–368.
 - [28] C. KUEHN, *Normal hyperbolicity and unbounded critical manifolds*, *Nonlinearity*, 27 (2014), p. 1351.
 - [29] C. KUEHN, *Multiple time scale dynamics*, vol. 191 of *Applied Mathematical Sciences*, Springer, 2015.
 - [30] C. KUEHN AND P. SZMOLYAN, *Multiscale geometry of the olsen model and non-classical relaxation oscillations*, *Journal of Nonlinear Science*, 25 (2015), pp. 583–629.
 - [31] I. LIZARRAGA, R. MARANGELL, AND M. WECHSELBERGER, *Slow unfoldings of contact singularities in singularly perturbed systems beyond the standard form*, *Journal of Nonlinear Science*, 30 (2020), pp. 3161–3198.
 - [32] I. LIZARRAGA, B. RINK, AND M. WECHSELBERGER, *Multiple timescales and the parametrisation method in geometric singular perturbation theory*, *Nonlinearity*, 34 (2021), p. 4163.
 - [33] I. LIZARRAGA AND M. WECHSELBERGER, *Computational singular perturbation method for nonstandard slow-fast systems*, *SIAM Journal on Applied Dynamical Systems*, 19 (2020), pp. 994–1028.
 - [34] J. LLIBRE, P. R. DA SILVA, AND M. A. TEIXEIRA, *Regularization of discontinuous vector fields on \mathbb{R}^3 via singular perturbation*, *Journal of Dynamics and Differential Equations*, 19 (2007), pp. 309–331.
 - [35] J. LLIBRE, P. R. DA SILVA, AND M. A. TEIXEIRA, *Study of singularities in nonsmooth dynamical systems via singular perturbation*, *SIAM Journal on Applied Dynamical Systems*, 8 (2009), pp. 508–526.
 - [36] A. MACHINA, R. EDWARDS, AND P. VAN DEN DRIESSCHE, *Singular dynamics in gene network models*, *SIAM Journal on Applied Dynamical Systems*, 12 (2013), pp. 95–125.
 - [37] A. MILIK AND P. SZMOLYAN, *Multiple time scales and canards in a chemical oscillator*, in *Multiple-time-scale dynamical systems*, Springer, 2001, pp. 117–140.
 - [38] J. MITRY, M. MCCARTHY, N. KOPELL, AND M. WECHSELBERGER, *Excitable neurons, firing threshold manifolds and canards*, *The Journal of Mathematical Neuroscience*, 3 (2013), pp. 1–32.
 - [39] N. PAGES, E. VERA-SIGÜENZA, J. RUGIS, V. KIRK, D. I. YULE, AND J. SNEYD, *A model of $ca\ 2+$ dynamics in an accurate reconstruction of parotid acinar cells*, *Bulletin of Mathematical Biology*, 81 (2019), pp. 1394–1426.
 - [40] E. PLAhte AND S. KJØGLUM, *Analysis and generic properties of gene regulatory networks with graded response functions*, *Physica D: Nonlinear Phenomena*, 201 (2005), pp. 150–176.
 - [41] A. POLITI, L. D. GASPERS, A. P. THOMAS, AND T. HÖFER, *Models of $ip\ 3$ and $ca\ 2+$ oscillations: frequency encoding and identification of underlying feedbacks*, *Biophysical journal*, 90 (2006), pp. 3120–3133.
 - [42] K.-L. ROBERTS, J. E. RUBIN, AND M. WECHSELBERGER, *Averaging, folded singularities, and torus canards: Explaining transitions between bursting and spiking in a coupled neuron model*, *SIAM Journal on Applied Dynamical Systems*, 14 (2015), pp. 1808–1844.
 - [43] J. E. RUBIN AND D. TERMAN, *Geometric singular perturbation analysis of neuronal dynamics*, in *Handbook of dynamical systems*, vol. 2, Elsevier, 2002, pp. 93–146.
 - [44] J. SNEYD AND M. FALCKE, *Models of the inositol trisphosphate receptor*, *Progress in biophysics and molecular biology*, 89 (2005), pp. 207–245.
 - [45] J. SNEYD, J. M. HAN, L. WANG, J. CHEN, X. YANG, A. TANIMURA, M. J. SANDERSON, V. KIRK, AND D. I. YULE, *On the dynamical structure of calcium oscillations*, *Proceedings of the National Academy of Sciences*, (2017), p. 201614613.
 - [46] T. VO, R. BERTRAM, AND M. WECHSELBERGER, *Multiple geometric viewpoints of mixed mode dynamics associated with pseudo-plateau bursting*, *SIAM Journal on Applied Dynamical Systems*, 12 (2013), pp. 789–830.
 - [47] M. WECHSELBERGER, *Geometric singular perturbation theory beyond the standard form*, in *Frontiers in Applied Dynamical Systems: Reviews and Tutorials*, vol. 6, Springer, 2020.

Appendix A. Proof of Theorem 5.9.

In this Appendix we prove Theorem 5.9. The main technique is the blow-up method developed in [8] in the formalism of [26, 27]. In Section A.1 we introduce a cylindrical blow-up of the degenerate line S_h , allowing us to resolve much of the degeneracy in (5.1), and extend the singular cycle Γ onto the blow-up cylinder. This allows for the presentation of a singular cycle with improved hyperbolicity properties, about which a Poincaré map is defined and analysed in Section A.2. We present a sequence of lemmas which will allow for a proof of Theorem 5.9, which is given in Section A.3. As part of this proof we rely on additional results obtained after the application of a successive (spherical) blow-up, which must be introduced in order to resolve additional degeneracy associated with a degenerate point that is identified following the cylindrical blow-up. This (successive) blow-up analysis is deferred to Section A.4 for expository reasons.

Remark A.1. The geometry and analysis of the relaxation cycles is similar in many respects to the autocatalytic relaxation oscillations studied in [37] and subsequently in [19].

A.1. Blow-up of the non-hyperbolic line S_h . We consider the extended system

$$(A.1) \quad \begin{aligned} \begin{pmatrix} h' \\ c' \end{pmatrix} &= g(h, c) + \epsilon G(h, c, \epsilon), \\ \epsilon' &= 0 \end{aligned}$$

obtained by adding the trivial equation $\epsilon' = 0$ to system (5.1), and define a weighted cylindrical blow-up by the transformation

$$(A.2) \quad r \geq 0, (\bar{c}, \bar{\epsilon}) \in S^1 \mapsto \begin{cases} c = r\bar{c}, \\ \epsilon = r^2\bar{\epsilon}, \end{cases}$$

which ‘blows up’ S_h to the cylinder $\{r = 0\} \times S^1 \times \mathbb{R}_+$. We work in two coordinate charts, defined via $K_1 : \bar{c} = 1$ and $K_2 : \bar{\epsilon} = 1$, for which we introduce chart-specific coordinates

$$(A.3) \quad K_1 : c = r_1, \epsilon = r_1^2 \epsilon_1, \quad K_2 : c = r_2 c_2, \epsilon = r_2^2.$$

Chart K_1 is referred to as an entry/exit chart, and chart K_2 is referred to as the ‘family rescaling’ chart. The transition maps between K_1 and K_2 are given by

$$(A.4) \quad \begin{aligned} \kappa_{12} : r_1 &= r_2 c_2, \quad \epsilon_1 = c_2^{-2}, \quad c_1 > 0, \\ \kappa_{21} : c_2 &= \epsilon_1^{-1/2}, \quad r_2 = r_1 \epsilon_1^{1/2}, \quad \epsilon_1 > 0. \end{aligned}$$

We will adopt some common notational conventions throughout the analysis. In particular, given a set \mathcal{A} , we denote its image in coordinate chart K_i by \mathcal{A}_i .

A.1.1. Dynamics in charts. In the family rescaling chart K_2 we have $r_2 = \sqrt{\epsilon} = \delta$. Following the time desingularisation $dt = \delta^{-3} dt_2$, which amounts to division of the vector field by δ^3 , one obtains system (5.9) in chart K_2 , except with the notation $C = c_2$, $\delta = r_2$. Since we have already studied this system in Section 5.2, we need not consider it further here.

Now consider the dynamics in chart K_1 . Differentiating the relevant expressions in (A.3) and applying a time desingularisation $dt = r_1^{-3} dt_1$ which amounts to division by r_1^3 , we obtain

$$(A.5) \quad \begin{aligned} h' &= r_1 \tau_{\max}^{-1} \left(\hat{h}_\infty(\epsilon_1) - h \right) (1 + \epsilon_1^2), \\ r_1' &= r_1 \left[\hat{J}_{\text{IPR}}(h, r_1, \epsilon_1) - \epsilon_1 \hat{\mathfrak{J}}_{\text{SERCA}}^+(r_1) + \epsilon_1^2 \hat{\mathfrak{J}}_{\text{SERCA}}^-(r_1) \right], \\ \epsilon_1' &= -2\epsilon_1 \left[\hat{J}_{\text{IPR}}(h, r_1, \epsilon_1) - \epsilon_1 \hat{\mathfrak{J}}_{\text{SERCA}}^+(r_1) + \epsilon_1^2 \hat{\mathfrak{J}}_{\text{SERCA}}^-(r_1) \right], \end{aligned}$$

where

$$(A.6) \quad \begin{aligned} \hat{h}_\infty(\epsilon_1) &:= \mathfrak{h}_\infty(r_1, r_1^2 \epsilon_1), & \hat{J}_{\text{IPR}}(h, r_1, \epsilon_1) &:= \frac{1}{r_1^4} J_{\text{IPR}}(h, r_1, r_1^2 \epsilon_1), \\ \hat{\mathfrak{J}}_{\text{SERCA}}^+(r_1) &:= \frac{1}{r_1^2} \mathfrak{J}_{\text{SERCA}}^+(r_1), & \hat{\mathfrak{J}}_{\text{SERCA}}^-(r_1) &:= \mathfrak{J}_{\text{SERCA}}^-(r_1), \end{aligned}$$

all extend smoothly to $r_1 = 0$ due to common factors of r_1 in their respective numerators. Note that the $(\cdot)'$ notation now denotes differentiation with respect to t_1 .

We identify two lines of equilibria

$$(A.7) \quad l_{h,1} = \{(h, 0, 0) : h \geq 0\}, \quad l_{c,1} = \{(0, r_1, 0) : r_1 \geq 0\},$$

as well as a smooth curve of equilibria

$$(A.8) \quad \mathcal{S}_1 = \{(\Psi(\epsilon_1), 0, \epsilon_1) : \epsilon_1 \geq 0\}, \quad \Psi(\epsilon_1) = \frac{A_{\text{SERCA}}}{A_{\text{IPR}} \gamma c_t} \epsilon_1 (1 - K \gamma^2 c_t^2 \epsilon_1).$$

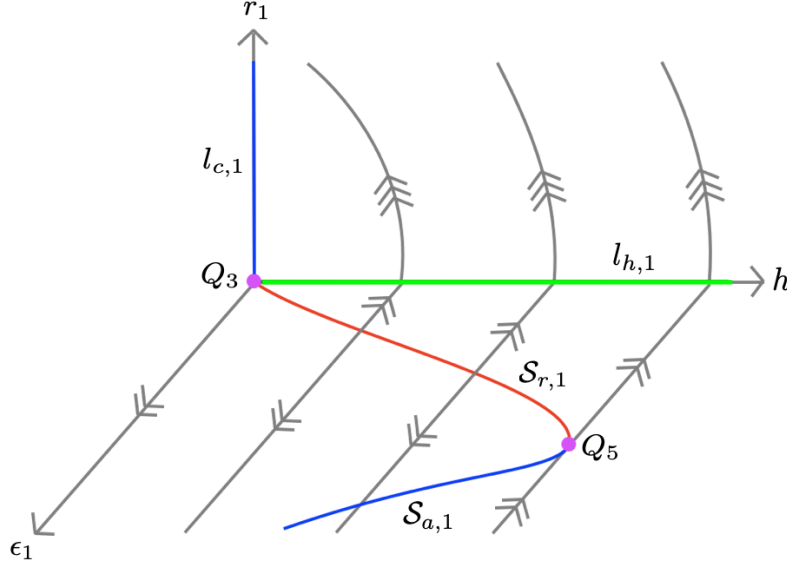


Fig. 8: Main dynamical features identified in the analysis in chart K_1 . Normally hyperbolic and attracting (repelling) manifolds of equilibria $l_{c,1}$ and $\mathcal{S}_{a,1}$ ($\mathcal{S}_{r,1}$) are shown in blue (red), and the line of saddle-type steady states $l_{h,1}$ is shown in green. The point Q_5 is the image of the regular jump point F in chart K_1 coordinates. The equilibrium Q_3 is nonhyperbolic and will require further blow-up; see Section A.4.

The line $l_{c,1}$ corresponds to the image of the attracting critical manifold S_c within chart K_1 . For $\epsilon_1 > 0$, the curve \mathcal{S}_1 coincides with the critical manifold identified in (5.13), which we denote here by \mathcal{S}_2 . The origin, which we denote by $Q_3 = (0, 0, 0)$, lies at the intersection of all three curves, and the regular fold point F in equation (5.15) is identified as a fold point Q_5 with chart K_1 coordinates

$$Q_5 = (h_f, r_{f,1}, \epsilon_{f,1}) = \left(\frac{A_{\text{SERCA}}}{4K A_{\text{IPR}} \gamma^3 c_t^3}, 0, \frac{1}{2K \gamma^2 c_t^2} \right).$$

The point Q_5 divides \mathcal{S}_1 into normally hyperbolic branches as $\mathcal{S}_1 = \mathcal{S}_{a,1} \cup \{Q_5\} \cup \mathcal{S}_{r,1}$, where

$$\mathcal{S}_{a,1} = \{(\Psi(\epsilon_1), 0, \epsilon_1) : \epsilon_1 > \epsilon_{f,1}\}, \quad \mathcal{S}_{r,1} = \{(\Psi(\epsilon_1), 0, \epsilon_1) : \epsilon_1 < \epsilon_{f,1}\};$$

see Figure 8. The following result describes stability properties of $l_{h,1}$, $l_{c,1}$, $\mathcal{S}_{a,1}$, $\mathcal{S}_{r,1}$ and Q_3 .

LEMMA A.2. *The following hold for system (A.1):*

- (i) *The line $l_{h,1} \setminus Q_3$ is partially hyperbolic and attracting, with eigenvalues $\lambda = -r_1 \tau_{\max}^{-1}, 0, 0$.*
- (ii) *The line $l_{h,1} \setminus Q_3$ is normally hyperbolic and saddle-type, with eigenvalues $\lambda = -2A_{\text{IPR}} \gamma c_t h, A_{\text{IPR}} \gamma c_t h, 0$. For each $b = \{(0, \alpha, 0)\} \in l_{h,1} \setminus Q_3$, the corresponding one-dimensional stable manifold $W^s(b)$ is contained within the line $h = b, r_1 = 0, \epsilon_1 \geq 0$.*
- (iii) *The critical manifolds $\mathcal{S}_{a,1}, \mathcal{S}_{r,1}$ are normally hyperbolic and attracting, respectively repelling.*
- (iv) *The point Q_3 is a nilpotent singularity, with eigenvalues $\lambda = 0, 0, 0$.*

Proof. Statements (i), (iii), (iv) and the first assertion in (ii) can be shown by direct calculations following linearisation of the system (A.5). To see that the stable manifold $W^s(b)$ for a given base point $b = \{(0, \alpha, 0)\} \in l_{h,1} \setminus Q_3$ lies within the line $h = \alpha, r_1 = 0, \epsilon_1 \geq 0$, consider the system obtained from (A.5) by restricting to the invariant plane $\{r_1 = 0\}$ (i.e., to the cylinder):

$$(A.9) \quad \begin{aligned} h' &= 0, \\ \epsilon_1' &= -2\epsilon_1 A_{\text{IPR}} \gamma c_t \left(h - \frac{A_{\text{SERCA}}}{A_{\text{IPR}} \gamma c_t} \epsilon_1 (1 - K \gamma^2 c_t^2 \epsilon_1) \right). \end{aligned}$$

The result follows from the observation that each line $h = \alpha, \epsilon_1 \geq 0$ is invariant under the flow induced by (A.9), with dynamics governed by

$$(A.10) \quad \epsilon_1' = -2\epsilon_1 A_{\text{IPR}} \gamma c_t \alpha + O(\epsilon_1^2). \quad \square$$

The results in Lemma A.2 lead to the following result.

LEMMA A.3. *Fix $\nu_+ > \nu_- > 0$ and $\eta > 0$. For η sufficiently small, system (A.1) has a two-dimensional center manifold*

$$M_1 = \left\{ (\hat{h}_\infty(\epsilon_1), r_1, \epsilon_1) : r_1 \in [\nu_-, \nu_+], \epsilon_1 \in [0, \eta] \right\},$$

containing the line of equilibria $l_{c,1}$ as the restriction $M_1|_{\epsilon_1=0}$. Moreover, there exists a stable foliation \mathcal{F}_1 with base M_1 and one-dimensional fibers. The contraction along \mathcal{F}_1 in a time interval of length t is stronger than e^{ct} for any $0 < c < \nu_-/\tau_{\text{max}}$, and the flow on M_1 is strictly decreasing in the variable r_1 .

Proof. Existence of a two-dimensional strongly attracting center manifold M_1 containing $l_{c,1}$ follows from Lemma A.2 and center manifold theory, and the existence of a stable foliation with exponential contraction follows from Fenichel theory.

To show that the flow on M_1 is strictly decreasing in the variable r_1 , we restrict equations (A.5) to M_1 , obtaining the system

$$(A.11) \quad \begin{aligned} r_1' &= - \left(\frac{V_s}{K_s^2 + r_1^2} \right) r_1 \epsilon_1 + O(r_1 \epsilon_1^2), \\ \epsilon_1' &= \left(\frac{2V_s}{K_s^2 + r_1^2} \right) \epsilon_1^2 + O(\epsilon_1^3). \end{aligned}$$

For $\eta > 0$ sufficiently small, $r_1' < 0$ as claimed. □

A.1.2. An improved singular cycle Γ . Our analysis thus far leads to the dynamics sketched in Figure 9. We have two lines of steady states (l_h and l_c), a folded critical manifold \mathcal{S} on the cylinder, and distinguished points $Q_i, i = 1, \dots, 5$ given in chart K_1 coordinates by $Q_1 = (h_f, 0, 0)$, $Q_2 = (0, r_{d,1}, 0)$, $Q_3 = (0, 0, 0)$, $Q_4 = (0, 0, \epsilon_{l,1})$ and $Q_5 = (h_f, 0, \epsilon_{f,1})$. The location of point Q_4 is given explicitly by $\epsilon_{l,1} = 1/K\gamma^2 c_t^2$. We do not give an explicit location for point Q_2 , noting simply that $r_{d,1} > 0$ by Lemma (A.4) below. Taking the points Q_i as concatenation points allows for the construction of a singular relaxation cycle

$$\Gamma = \Gamma_1 \cup \Gamma_2 \cup \Gamma_3 \cup \Gamma_4 \cup \Gamma_5,$$

where, again in K_1 coordinates, we define

$$(A.12) \quad \begin{aligned} \Gamma_1 &= \Gamma_l, \\ \Gamma_2 &= \{(0, r_1, 0) : r_1 \in (0, r_{d,1})\}, \\ \Gamma_3 &= \{(0, 0, \epsilon_1) : \epsilon_1 \in (0, \epsilon_{l,1})\}, \\ \Gamma_4 &= \{(\Psi(\epsilon_1), 0, \epsilon_1) : \epsilon_1 \in (\epsilon_{f,1}, \epsilon_{l,1})\}, \\ \Gamma_5 &= \{(h_f, 0, \epsilon_1) : \epsilon_1 \in (0, \epsilon_{f,1})\}, \end{aligned}$$

see Figure 9. In order to prove Theorem (5.9), we need to show that Γ persists for $\epsilon \ll 1$ sufficiently small.

A.2. Poincaré map. We define a number of sections transversal to Γ , expressed in chart K_1 coordinates as follows:

$$(A.13) \quad \begin{aligned} \Sigma_1 &= \{(h, \rho_1, \epsilon_1) : |h - h_f| \leq \alpha_1, \epsilon_1 \in [0, \beta_1]\}, \\ \Sigma_2 &= \{(\nu_1, r_1, \epsilon_1) : |r_1 - r_{d,1}| \leq \rho_2, \epsilon_1 \in [0, \beta_2]\}, \\ \Sigma_3 &= \{(h, \rho_1, \epsilon_1) : |h| \leq \alpha_2, \epsilon_1 \in [0, \beta_3]\}, \\ \Sigma_4 &= \{(h, r_1, \beta_2) : |h| \leq \alpha_2, r_1 \in [0, \rho_3]\}, \\ \Sigma_5 &= \{(h, r_1, \epsilon_{f,1} + \beta_3) : |h - h_f| \leq \alpha_3, r_1 \in [0, \rho_4]\}, \\ \Sigma_6 &= \{(h, r_1, \beta_2) : |h - h_f| \leq \alpha_1, r_1 \in [0, \rho_5]\}, \end{aligned}$$

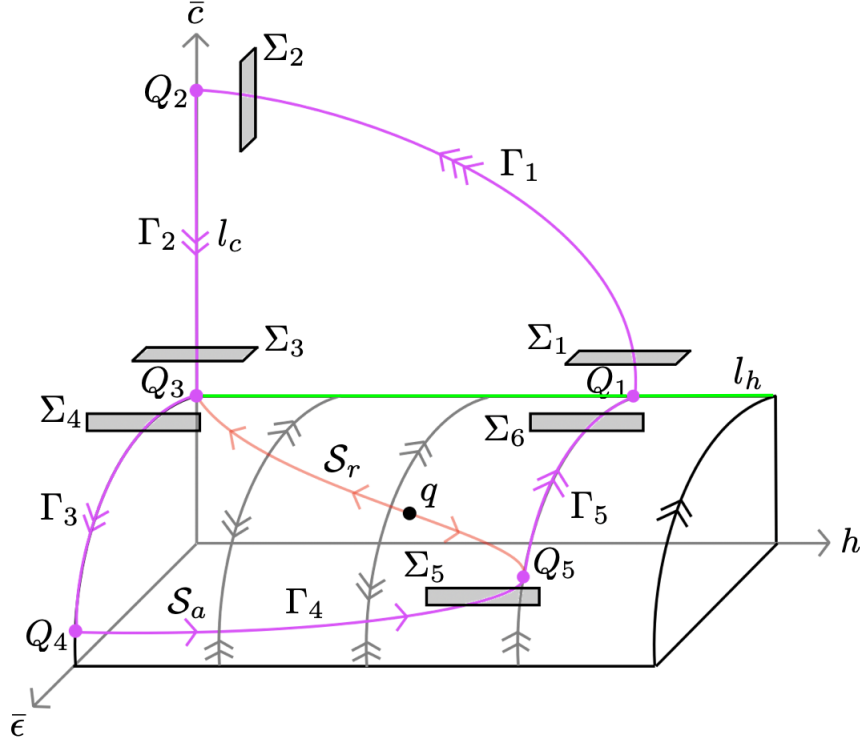


Fig. 9: Main dynamical features after cylindrical blow-up of the degenerate line S_h . The dynamics observed in the analysis in scaling regime (R1) correspond to the dynamics bounded ‘above’ the cylinder, while the dynamics in scaling regime (R2) appear on the cylinder itself. The singular relaxation cycle $\Gamma = \Gamma_1 \cup \Gamma_2 \cup \Gamma_3 \cup \Gamma_4 \cup \Gamma_5$ is shown in magenta, and the segments Σ_i , $i = 1, \dots, 6$ used to define the Poincaré map in Section A.2 are also shown. Although both are indicated with double arrows, we note that the speed along Γ_2 is not the same as the speed along Γ_5 (see Remark 5.7).

see Figure 9. We define the Poincaré map $\pi : \Sigma_1 \rightarrow \Sigma_1$ induced by the flow of (A.1) by a composition of component maps

$$(A.14) \quad \pi = \pi_6 \circ \pi_5 \circ \pi_4 \circ \pi_2 \circ \pi_2 \circ \pi_1,$$

where $\pi_i : \Sigma_i \rightarrow \Sigma_{i+1}$ for $i \in \{1, \dots, 5\}$, and $\pi_6 : \Sigma_6 \rightarrow \Sigma_1$. We consider each of the transition maps π_i in turn. Except in the case of the map π_1 , the arguments presented are similar to those in [19].

The map $\pi_1 : \Sigma_1 \rightarrow \Sigma_2$. Boundedness argument. We consider the map $\pi_1 : \Sigma_1 \rightarrow \Sigma_2$ in the original coordinates (h, c, ϵ) of the extended system (A.1). Note that in these coordinates,

$$(A.15) \quad \begin{aligned} \Sigma_1 &= \{(h, \rho_1, \epsilon) : |h - h_f| \leq \alpha_1, \epsilon \in [0, \rho_1^2 \beta_1]\}, \\ \Sigma_2 &= \{(\nu_1, c, \epsilon) : |c - c_d| \leq \rho_2, \epsilon \in [0, (c_d + \rho_2)^2 \beta_2]\}, \end{aligned}$$

where $c_d = r_{d,1}$. The transition map π_1 is characterised by the following result.

LEMMA A.4. *For ϵ sufficiently small, the map π_1 is a well-defined diffeomorphism.*

Proof. We consider the auxiliary problem to the layer problem for the extended system (A.1),

$$(A.16) \quad \begin{pmatrix} h' \\ c' \\ \epsilon' \end{pmatrix} = \begin{pmatrix} -\tau_{\max}^{-1} \\ \mathfrak{J}_{\text{IPR}}^{(0)}(h, c) \\ 0 \end{pmatrix},$$

obtained after making the time desingularisation $dt = c^{-4}h^{-1}dT$. Note that the dash notation now refers to differentiation by the new time T . System (A.16) is equivalent to the layer problem (A.1)| $_{\epsilon=0}$ on the relevant domain $h, c > 0$. The transition time T_{h_0} for a trajectory with initial condition $(h_0, \rho_1, 0) \in \Sigma_1$ to reach a point $(\nu_1, \tilde{c}, 0) \in \Sigma_2$ can be determined by integrating the equation for h' . We obtain

$$h(T) = -\tau_{\max}^{-1}T + h_0 \quad \implies \quad T_{h_0} = \tau_{\max}(h_0 - \nu_1),$$

where ν_1 is chosen so that $T_{h_0} > 0$. Now fix a compact box

$$R = \{(h, c) : h \in [h_-, h_+], c \in [c_-, c_+]\},$$

such that $h_-, c_- > 0$, and $\Sigma_{1,2} \subset R$. We obtain an upper bound for the corresponding transition time t_{h_0} for the layer problem (A.1)| $_{\epsilon=0}$ via

$$t_{h_0} = \int_0^{T_{h_0}} dt = \int_0^{T_{h_0}} \frac{1}{c^4(T)h(T)} dT \leq \frac{T_{h_0}}{c_-^4 h_-} < \infty. \quad \square$$

It follows that $\pi_1|_{\epsilon=0}$ is a well-defined diffeomorphism. Since the flow in R is regular, it follows by regular perturbation theory and the flowbox theorem that for $\epsilon \ll 1$ sufficiently small, π_1 is also a well-defined diffeomorphism.

The map $\pi_2 : \Sigma_2 \rightarrow \Sigma_3$. Fenichel theory in (h, c, ϵ) -coordinates. The map π_2 is characterised by the following result, stated in terms of the coordinates (h, c, ϵ) .

LEMMA A.5. *For $\epsilon > 0$ sufficiently small, the map π_2 is well-defined and the c -component of the map is contracting with rate $e^{-a_2/\epsilon}$, for a constant $a_2 > 0$.*

Proof. Given $\nu_1 > 0$ sufficiently small, Fenichel theory implies that solutions with initial conditions in Σ_2 are exponentially attracted to their base points on the slow manifold $S_{c,\epsilon}$ described in Lemma 5.5. Trajectories follow the slow flow on $S_{c,\epsilon}$ until they reach Σ_3 . Hence the map $\pi_2 : \Sigma_2 \rightarrow \Sigma_3$ is well-defined. Exponential contraction in the c -component follows by Fenichel theory [10]. \square

The map $\pi_3 : \Sigma_3 \rightarrow \Sigma_4$. Spherical blow-up of Q_3 . Let $R_3 \subset \Sigma_3$ be an arbitrarily small rectangle centered at the point $(0, \rho_1, 0)$ in chart K_1 coordinates, i.e., at the intersection $\Gamma \cap \Sigma_3$. The transition map $\pi_3 : \Sigma_3 \rightarrow \Sigma_4$ is characterised by the following result.

LEMMA A.6. *Given $\rho_1 > 0$ and $R_3 \subset \Sigma_3$ sufficiently small, the restricted map $\pi_3|_{R_3} = \pi_{3,R_3}$ is C^1 -smooth with the following properties:*

- (i) *The extension of the manifold M described in Lemma A.3 intersects Σ_4 in a C^1 -curve σ_4 , which is tangent to $r_1 = 0$.*
- (ii) *Each restricted map $\pi_{3,R_3}|_{\epsilon_1=\text{const}}$ is a strong contraction with rate e^{-a_3/ϵ_1} for a constant $a_3 > 0$*
- (iii) *The image $\pi_3(R_3)$ is an exponentially thin wedge about σ_4 in Σ_4 .*

Proof. The proof relies on a spherical blow-up of the nilpotent point Q_3 . For expository reasons, we defer the proof to Appendix A.4. \square

The map $\pi_4 : \Sigma_4 \rightarrow \Sigma_5$. Fenichel theory in chart K_2 . The transition map $\pi_4 : \Sigma_4 \rightarrow \Sigma_5$ is analysed in chart K_2 . We may use the fact that $r_2 = \delta$, however, in order to describe the result in terms of the regime (R2) analysis given in Section 5.2.

LEMMA A.7. *Given fixed $\rho_1 > 0$, there exists $\beta_2 > 0$ such that the map π_4 is well-defined with the following properties:*

- (i) *Each restricted map $\pi_4|_{\delta=\text{const}}$ is a strong contraction with rate $O(e^{-a_4/\epsilon^2})$ for a constant $a_4 > 0$.*
- (ii) *The image $\pi_4(\Sigma_4)$ is an exponentially thin wedge in Σ_5 , which is exponentially close to the smooth curve formed by the intersection $\mathcal{S}_{a,\delta,2} \cap \Sigma_5$.*

Proof. For sufficiently small $\beta_2 > 0$ our analysis in regime (R2) in Section 5.2, in particular Lemma 5.8, implies that solutions with initial conditions in Σ_4 are exponentially attracted to their base points on $\mathcal{S}_{a,\delta,2}$, after which they follow the slow flow and intersect Σ_5 transversally. Hence $\pi_4 : \Sigma_4 \rightarrow \Sigma_5$ is well-defined.

Statements (i)-(ii) follow by the exponential contractiveness of the slow manifolds $\mathcal{S}_{a,\delta,2}$. In particular, $O(e^{-a_4/\epsilon^2})$ contraction follows since solutions track the slow flow on $\mathcal{S}_{a,\delta,2}$ for $O(1)$ times on the infra-slow time-scale $\tilde{\tau} = \epsilon^2 t$; see again Remark 5.7. \square

The map $\pi_5 : \Sigma_5 \rightarrow \Sigma_6$. Flow past the fold in chart K_2 . The transition map $\pi_5 : \Sigma_5 \rightarrow \Sigma_6$ is also considered in chart K_2 . In these coordinates we have

$$(A.17) \quad \begin{aligned} \Sigma_5 &= \left\{ \left(h, \frac{1}{(\epsilon_{f,1} + \beta_3)^2}, r_2 \right) : |h - h_{f,2}| \leq \alpha_3, r_2 \in [0, (\epsilon_{f,1} + \beta_3)^2 \rho_4] \right\}, \\ \Sigma_6 &= \left\{ \left(h, \frac{1}{\sqrt{\beta_2}}, r_2 \right) : |h - h_{f,2}| \leq \alpha_1, r_2 \in [0, \sqrt{\beta_2} \rho_5] \right\}. \end{aligned}$$

We obtain the following result.

LEMMA A.8. *Fix the section Σ_5 sufficiently small. Then for all $r_2 > 0$ sufficiently small, the transition map π_5 is well-defined. In particular, the image $\pi_5(\Sigma_5) \subset \Sigma_6$ is exponentially narrow in the h -coordinate ($O(e^{-a_5/r_2})$ for some $a_5 > 0$), and centered about the value $h = h_{f,2} + O(r_2^{2/3})$.*

Proof. For $r_2 > 0$ sufficiently small, solutions with initial conditions in Σ_5 are exponentially attracted to their base points on the slow manifolds $\mathcal{S}_{a,\delta,2}$ described in Lemma 5.8. Lemma 5.8 also implies the extension of $\mathcal{S}_{a,\delta,2}$ (and nearby trajectories) through the neighbourhood of the fold point Q_5 , see again Figure 6. After leaving a neighbourhood of the fold, solutions follow the fast flow for finite time before intersecting Σ_6 . This shows that π_5 is well-defined. Exponential contraction follows from Fenichel theory [10] and the exponential contractiveness undergone in the neighbourhood of Q_f . Finally, the estimate for the h -component follows from Lemma 5.8 and regular perturbation theory. \square

The map $\pi_6 : \Sigma_6 \rightarrow \Sigma_1$. Hyperbolic transition near l_h . The analysis of the map $\pi_6 : \Sigma_6 \rightarrow \Sigma_1$ is carried out in chart K_1 . Let $p_0 = (h_f, 0, \beta_2)$ denote the point of intersection at $\Gamma \cap \Sigma_1$, and let $R_6 \subset \Sigma_6$ be an arbitrarily small (but fixed) rectangle centered at p_0 . For notational simplicity, we rewrite system (A.5) as

$$(A.18) \quad \begin{aligned} h' &= r_1 \phi(h, \epsilon_1), \\ r_1' &= r_1 \psi(h, r_1, \epsilon_1), \\ \epsilon_1' &= -2\epsilon_1 \psi(h, r_1, \epsilon_1), \end{aligned}$$

where

$$(A.19) \quad \begin{aligned} \phi(h, \epsilon_1) &= \tau_{\max}^{-1} \left(\hat{h}_\infty(\epsilon_1) - h \right) (1 + \epsilon_1^2), \\ \psi(h, r_1, \epsilon_1) &= \hat{J}_{\text{IPR}}(h, r_1, \epsilon_1) - \epsilon_1 \hat{\mathcal{J}}_{\text{SERCA}}^+(r_1, \epsilon_1) + \epsilon_1^2 \hat{\mathcal{J}}_{\text{SERCA}}^-(r_1, \epsilon_1). \end{aligned}$$

For ease of computations, we translate the point $Q_1 = (h_f, 0, 0)$ to the origin via the translation $\tilde{h} = h - h_f$, obtaining the system

$$(A.20) \quad \begin{aligned} \tilde{h}' &= r_1 \tilde{\phi}(\tilde{h}, \epsilon_1), \\ r_1' &= r_1 \tilde{\psi}(\tilde{h}, r_1, \epsilon_1), \\ \epsilon_1' &= -2\epsilon_1 \tilde{\psi}(\tilde{h}, r_1, \epsilon_1), \end{aligned}$$

where $\tilde{\phi}(\tilde{h}, \epsilon_1) = \phi(\tilde{h} + h_f, \epsilon_1)$ and $\tilde{\psi}(\tilde{h}, r_1, \epsilon_1) = \psi(\tilde{h} + h_f, r_1, \epsilon_1)$. Since $\tilde{\psi}(0, 0, 0) = p^2 k_{\text{IPR}} \gamma c_t h_f / k_\beta K_c^4 K_p^2 > 0$, we may consider the equivalent system obtained after division by this term:

$$(A.21) \quad \begin{aligned} \tilde{h}' &= r_1 \left(\frac{\tilde{\phi}(\tilde{h}, \epsilon_1)}{\tilde{\psi}(\tilde{h}, r_1, \epsilon_1)} \right), \\ r_1' &= r_1, \\ \epsilon_1' &= -2\epsilon_1. \end{aligned}$$

System (A.21) has a non-hyperbolic equilibrium at $(0, 0, 0)$ with eigenvalues $0, 1, -2$. The transition map $\pi_6 : \Sigma_2 \rightarrow \Sigma_1$ is characterised by the following result.

LEMMA A.9. For $\beta_2 > 0$ sufficiently small and a sufficiently small rectangle $R_6 \subset \Sigma_6$ centered at p_0 , the restricted transition map $\pi_6|_{R_6} = \pi_{6,R_6}$ is well-defined and given by

$$(A.22) \quad \pi_6|_{R_6} : (h, r_1, \beta_2) \mapsto \left(h_f + O(r_1, h - h_f), \rho_1, \beta_2 \left(\frac{r_1}{\rho_1} \right)^2 \right).$$

Proof. We consider a solution $(\tilde{h}, \epsilon_1, r_1)(t)$ of (A.21) which satisfies

$$(\tilde{h}, r_1, \epsilon_1)(0) = (\tilde{h}_{in}, r_{1,in}, \beta_2), \quad (\tilde{h}, r_1, \epsilon_1)(T) = (\tilde{h}_{out}, \rho_1, \epsilon_{1,out}).$$

Direct integration yields $\epsilon_1(t) = \beta_2 e^{-2t}$ and $r_1(t) = r_{1,in} e^t$, which leads to an expression for the transition time

$$T = \ln \left(\frac{\rho_1}{r_{1,in}} \right),$$

proving that

$$\pi_6 : (h_{1,in}, r_{1,in}, \beta_2) \mapsto \left(h_{1,out}, \rho_1, \beta_2 \left(\frac{r_{1,in}}{\rho_1} \right)^2 \right).$$

Expanding the equation for \tilde{h}' in (A.21) about $(0, 0, 0)$ gives

$$\tilde{h}' = -ar_1 + O\left(r_1 \tilde{h}, r_1 \epsilon_1^2\right),$$

where $a = (\tau_{\max} A_{\text{IPR}} \gamma c_t)^{-1} > 0$. Since the expression for \tilde{h}' in (A.21) is C^1 , the order is well-behaved with respect to integration. The expression in (A.22) follows after direct integration and a coordinate translation $h = \tilde{h} + h_f$ which undoes the earlier transformation. \square

A.3. Proof of Theorem 5.9.

Proof. By the analysis presented in Section A.2, the Poincaré map $\pi : \Sigma_1 \rightarrow \Sigma_1$ defined by the composition in (A.14) is well-defined. Note that one must also include coordinate changes between charts in expression (A.14).

Because ϵ is a constant of the motion in (A.1), the lines $\epsilon = \text{const}$ are invariant under π . Since the relevant components of the restricted maps $\pi_i|_{\{\epsilon=\text{const}\}}$ are exponentially contracting for $i \in \{2, 3, 4, 5\}$, it follows that the h -component of the restricted map $\pi|_{\{\epsilon=\text{const}\}}$ is also exponentially contracting. By the contraction mapping theorem, each $\pi|_{\{\epsilon=\text{const}\}}$ has a unique fixed point corresponding to an exponentially attracting periodic orbit Γ_ϵ , and the family Γ_ϵ converges in the Hausdorff distance to the singular cycle Γ as $\epsilon \rightarrow 0$. Theorem 5.9 follows after applying the blow-down transformation associated with the map (A.2). The $O(\epsilon^{1/3})$ separation follows from Lemma (A.8) after applying $r_2 = \sqrt{\epsilon}$; see again the discussion immediately following the statement of Theorem 5.9. The $-\kappa/\epsilon^2$ bound on the Floquet exponent follows from Lemma A.2. \square

A.4. Proof of Lemma A.6. In this section we prove Lemma A.6. We start in K_1 coordinates with system (A.18), and drop the subscripts for notational convenience, i.e., we consider

$$(A.23) \quad \begin{aligned} h' &= r\phi(h, \epsilon), \\ r' &= r\psi(h, r, \epsilon), \\ \epsilon' &= -2\epsilon\psi(h, r, \epsilon), \end{aligned}$$

with ϕ and ψ as defined in (A.19). We are interested in the dynamics near the nilpotent singularity $Q_3 = (0, 0, 0)$, where the Jacobian has an eigenvalue $\lambda = 0$ of multiplicity three; recall Lemma A.2. In order to resolve this, we define a spherical blow-up by the transformation

$$(A.24) \quad s \geq 0, \quad (\bar{h}, \bar{r}, \bar{\epsilon}) \in S^2 \mapsto \begin{cases} h = s\bar{h}, \\ r = s\bar{r}, \\ \epsilon = s\bar{\epsilon}, \end{cases}$$

which maps the point Q_3 to the sphere $\{s = 0\} \times S^2$. We work in coordinate charts defined via $\mathcal{K}_1 : \bar{r} = 1$ and $\mathcal{K}_2 : \bar{\epsilon} = 1$, with chart-specific coordinates

$$(A.25) \quad \begin{aligned} \mathcal{K}_1 : h &= s_1 h_1, \quad r = s_1, \quad \epsilon = s_1 \epsilon_1, \\ \mathcal{K}_2 : h &= s_2 h_2, \quad r = s_2 r_2, \quad \epsilon = s_2. \end{aligned}$$

The transition maps between charts \mathcal{K}_1 and \mathcal{K}_2 are given by

$$(A.26) \quad \begin{aligned} \kappa_{12} : h_1 &= r_2^{-1} h_2, \quad s_1 = r_2 s_2, \quad \epsilon_1 = r_2^{-1}, \\ \kappa_{21} : h_2 &= \epsilon_1^{-1} h_1, \quad r_2 = \epsilon_1^{-1}, \quad s_2 = s_1 \epsilon_1. \end{aligned}$$

Note that in chart \mathcal{K}_1 and \mathcal{K}_2 coordinates, $\Sigma_3 \subset \{s_1 = \rho_1\}$ and $\Sigma_4 \subset \{s_2 = \beta_2\}$.

Chart \mathcal{K}_1 dynamics. After a suitable desingularisation (division by s_1), we obtain the following equations in chart \mathcal{K}_1 :

$$(A.27) \quad \begin{aligned} h_1' &= \bar{\phi}_1(h_1, \epsilon_1, s_1) - h_1 \bar{\psi}(h_1, \epsilon_1, s_1), \\ \epsilon_1' &= -3\epsilon_1 \bar{\psi}_1(h_1, \epsilon_1, s_1), \\ s_1' &= s_1 \bar{\psi}_1(h_1, \epsilon_1, s_1), \end{aligned}$$

where $\bar{\phi}_1(h_1, \epsilon_1, s_1) = s_1^{-1} \phi(s_1 h_1, s_1 \epsilon_1)$ and $\bar{\psi}_1(h_1, \epsilon_1, s_1) = s_1^{-1} \psi(s_1 h_1, s_1 \epsilon_1)$ are well-defined for $s_1 = 0$ due to a common factor of s_1 in the respective numerators. System (A.27) has a line of steady states

$$L_{c,1} = \{(0, 0, s_1) : s_1 \geq 0\},$$

and we denote the endpoint of $L_{c,1}$ by $p_c = (0, 0, 0) \in L_{c,1}$. We also identify the following invariant subspaces:

- (i) the plane $\epsilon_1 = 0$;
- (ii) the plane $r_1 = 0$;
- (iii) the h_1 -axis $r_1 = \epsilon_1 = 0, h_1 \geq 0$;
- (iv) the ϵ_1 -axis, which we denote by

$$(A.28) \quad \gamma_1 = \{(0, \epsilon_1, 0) : \epsilon_1 \geq 0\}.$$

For the purpose of stating the following result, we also write the rectangle $R_3 \subset \Sigma_3$ in chart \mathcal{K}_1 coordinates:

$$R_3 = \{(h, \epsilon_1, \rho_1) : |h| \leq \bar{\alpha}, \epsilon_1 \in [0, \bar{\alpha}]\}.$$

LEMMA A.10. *The following holds for system (A.27):*

- (i) *The line $L_{c,1}$ is normally hyperbolic and attracting, with eigenvalues $\lambda = -\tau_{\max}^{-1}, 0, 0$.*
- (ii) *There exists an attracting two-dimensional center manifold \mathcal{M}_1 with graph representation*

$$(A.29) \quad h_1 = K_h^4 s_1 \epsilon_1^2 + O(s_1^2 \epsilon_1^2),$$

containing $L_{c,1}$ and the invariant ϵ_1 -axis as restrictions $\mathcal{M}_1|_{\epsilon_1=0}$ and $\mathcal{M}_1|_{s_1=0}$ respectively. The manifold \mathcal{M}_1 can be chosen to be the continuation of the manifold M_1 in Lemma A.3 under the flow, and the variable ϵ_1 is strictly increasing on $\mathcal{M}_1 \setminus L_{c,1}$.

Proof. Statement (i) follows after linearisation of system (A.27), and existence of an attracting two-dimensional center manifold \mathcal{M} at p_c follows from center manifold theory. The graph representation (A.29) can be determined by standard matching arguments. Restricting system (A.27) to $\mathcal{M}_1 \setminus L_{c,1}$, we obtain

$$(A.30) \quad \begin{aligned} \epsilon_1' &= 3A_{\text{SERCA}} \epsilon_1^2 + O(\epsilon_1^3), \\ s_1' &= A_{\text{SERCA}} s_1 \epsilon_1 + O(s_1 \epsilon_1^2). \end{aligned}$$

and hence $\epsilon_1' > 0$, since $\epsilon_1 > 0$ on $\mathcal{M}_1 \setminus L_{c,1}$. □

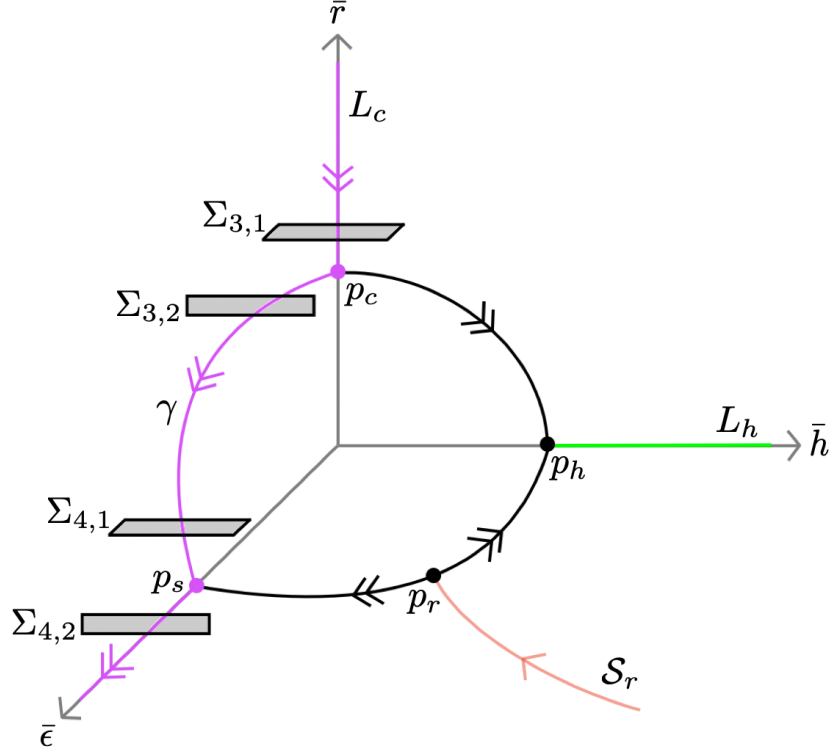


Fig. 10: Dynamics following spherical blow-up of Q_3 . The relevant part of the singular relaxation cycle is shown in purple. Also shown are the transversal segments $\Sigma_{3,i}$ and $\Sigma_{4,i}$, $i = 1, 2$ used in the construction of the map $\pi_3 : \Sigma_3 \rightarrow \Sigma_3$.

Chart \mathcal{K}_2 dynamics. After a suitable desingularisation (division by s_2), the dynamics in chart \mathcal{K}_2 are governed by

$$(A.31) \quad \begin{aligned} h'_2 &= r_2 \bar{\phi}_2(h_2, r_2, s_2) + 2h_2 \bar{\psi}_2(h_2, r_2, s_2), \\ r'_2 &= 3r_2 \bar{\psi}_2(h_2, r_2, s_2), \\ s'_2 &= -2s_2 \bar{\psi}_2(h_2, r_2, s_2), \end{aligned}$$

where $\bar{\phi}_2(h_2, r_2, s_2) = s_2^{-1} \phi(s_2 h_2, s_2)$ and $\bar{\psi}_2(h_2, r_2, s_2) = s_2^{-1} \psi(s_2 h_2, s_2 r_2, s_2)$, which are well-defined for $s_2 = 0$ due to a common factor of s_2 in the respective numerators. System (A.31) has an equilibrium $p_s = (0, 0, 0)$, and the following invariant subspaces:

- (i) the plane $r_2 = 0$;
- (ii) the plane $s_2 = 0$;
- (iii) the h_2 -axis $r_2 = s_2 = 0, h_2 \geq 0$;
- (iv) the r_2 -axis, which we denote by

$$(A.32) \quad \gamma_2 = \{(0, r_2, 0) : r_2 \geq 0\};$$

- (v) the s_2 -axis $h_2 = r_2 = 0, s_2 \geq 0$.

We obtain the following result.

LEMMA A.11. *The following hold for system (A.31):*

- (i) *The equilibrium p_s is hyperbolic with eigenvalues given by $\lambda = -2A_{SERCA}, -3A_{SERCA}, 2A_{SERCA}$, with corresponding eigenvectors $(1, 0, 0)^T$, $(0, 1, 0)^T$, and $(0, 0, 1)^T$. The unstable manifold $W^u(p_s)$ lies within the s_2 -axis $h_2 = r_2 = 0, s_2 \geq 0$.*

(ii) The invariant line γ_1 in (A.28) coincides with the invariant line γ_2 in (A.32) where domains overlap.

Proof. The first part of statement (i) follows after linearisation of system (A.31). The fact that $W^u(p_s)$ lies within the s_2 -axis follows from the form of the equations restricted to $h_2 = r_2 = 0$, namely

$$s_2' = -2s_2\bar{\psi}_2(0, 0, s_2) = \frac{2V_s s_2}{K_s^2 + s_2^2} + O(s_2^2) \geq 0.$$

Statement 2 follows by an application of the transition map κ_{12} in (A.26). \square

In particular, Lemma A.11 implies the existence of a heteroclinic orbit γ on the blown-up locus connecting p_c and p_s . The resulting (global) singular limit analysis is shown in Figure 10.

Remark A.12. Figure 10 shows objects that are not explicitly identified in our analysis, since they do not play an important role in the relevant dynamics. We simply note here that one can prove the existence of an additional (partially hyperbolic) equilibrium p_r corresponding to the endpoint of the (extension of the) repelling critical manifold \mathcal{S}_r in chart \mathcal{K}_2 . By looking in an additional chart $\bar{h} = 1$ one also identifies the image of the line of saddle-type steady states l_h , denoted L_h in Figure 10, which terminates at a point p_h on the blow-up sphere.

A.4.1. The map π_3 . In order to prove Lemma A.6, we consider the map $\pi_3 : \Sigma_3 \rightarrow \Sigma_4$ as a composition

$$\pi_3 = \pi_{4,1} \circ \pi_{3,2} \circ \pi_{3,1},$$

where $\pi_{3,1} : \Sigma_{3,1} \rightarrow \Sigma_{3,2}$, $\pi_{3,2} : \Sigma_{3,2} \rightarrow \Sigma_{4,1}$ and $\pi_{4,1} : \Sigma_{4,1} \rightarrow \Sigma_{4,2}$ denote transition maps induced by the flow. We consider each map in turn. The arguments presented are similar to those in [19, Appendix A].

The map $\pi_{3,1} : \Sigma_{3,1} \rightarrow \Sigma_{3,2}$. Extension of \mathcal{M} onto the blow-up sphere. Here we are interested in the dynamics near the point p_c . The analysis is carried out in chart \mathcal{K}_1 , and we define

$$\Sigma_3 = \Sigma_{3,1} = \left\{ (h_1, \epsilon_1, \rho_1) : |h_1| \leq \tilde{\alpha}_3, \epsilon_1 \in [0, \tilde{\beta}_3] \right\},$$

and

$$\Sigma_{3,2} = \left\{ (h_1, \rho_1, s_1) : |h_1| \leq \tilde{\alpha}_3, s_1 \in [0, \tilde{\beta}_3] \right\},$$

where $\tilde{\alpha}_3 := \alpha_2/\rho_1$ and $\tilde{\beta}_3 := \beta_3/\rho_1$. The following result describes the map $\pi_{3,1} : \Sigma_{3,1} \rightarrow \Sigma_{3,2}$.

LEMMA A.13. *Given $\tilde{\alpha}_3, \tilde{\beta}_3 > 0$ sufficiently small, the restricted transition map $\pi_{3,1}|_{R_3} = \pi_{3,1,R_3}$ is well-defined and C^1 with the following properties:*

(i) *The intersection $\mathcal{M}_1 \cap \Sigma_{3,2}$ is a smooth curve given by the graph*

$$h_1 = -K_h^4 \rho_1^2 s_1 + O(\rho_1^2 s_1^2).$$

(ii) *Restricted to lines $\epsilon_1 = \text{const}$ the map $\pi_{3,1,R_3}$ is exponentially contracting with rate $e^{-\tilde{a}_1/\epsilon_1}$ for a constant $\tilde{a}_1 > 0$.*

Proof. Statements (i) and (ii) follow immediately from Lemma A.3. \square

The map $\pi_{3,2} : \Sigma_{3,2} \rightarrow \Sigma_{4,1}$. Tracking \mathcal{M} over the blow-up sphere. We are interested here in the extension of the manifold \mathcal{M} in chart \mathcal{K}_1 . We define

$$\Sigma_{4,1} = \left\{ \left(h_1, \frac{1}{\beta_2}, s_1 \right) : |h_1| \leq \alpha_2, s_1 \in [0, \rho_3] \right\}.$$

The dynamics are summarised in the following result.

LEMMA A.14. *Given sufficiently small $\rho_1, \alpha_2, \beta_2 > 0$, the map $\pi_{3,2} : \Sigma_{3,2} \rightarrow \Sigma_{4,1}$ is a well-defined diffeomorphism. The intersection of the extension of \mathcal{M}_1 under the flow with $\Sigma_{4,1}$ is a smooth curve with tangent vector*

$$(A.33) \quad t_Q \approx \left(-K_h^4 \rho_1^2 \left(\frac{1 - 3A_{\text{SERCA}} \rho_1^2}{\rho_1 \beta_2} \right)^{1/3}, 0, \left(\frac{A_{\text{SERCA}} + \rho_1 \beta_2 - 1}{A_{\text{SERCA}} (1 - 3\rho_1)^2} \right)^{1/3} \right)^T$$

at Q .

Proof. The intersection $\gamma_1 \cap \Sigma_{3,2}$ occurs at $P = (0, \rho_1, 0)$, and the intersection $\gamma_1 \cap \Sigma_{4,1}$ occurs at $Q = (0, 1/\beta_2, 0)$. Since the flow from P to Q along γ_1 is regular, all solutions with initial conditions in $\Sigma_{3,2}$ reach $\Sigma_{4,1}$ in finite time if $\rho_1, \alpha_2, \beta_2 > 0$ are sufficiently small. It follows that $\pi_{3,2}$ is a well-defined diffeomorphism.

In order to understand the continuation of the manifold \mathcal{M}_1 , we compute the evolution of its tangent space along the line γ_1 . Note that in the parameterisation given in (A.28), $\epsilon = \rho_1$ corresponds to the point $P \in \Sigma_{3,2}$, and $\epsilon_1 = 1/\beta_2$ corresponds to the point $Q \in \Sigma_{4,1}$. The variational equations along γ_1 are

$$(A.34) \quad \begin{pmatrix} \delta h_1' \\ \delta \epsilon_1' \\ \delta s_1' \end{pmatrix} = \begin{pmatrix} A_{\text{SERCA}} \epsilon_1 - \tau_{\max}^{-1} & 0 & \tau_{\max}^{-1} K_h^4 \epsilon_1^2 \\ -3A_{\text{IPR}} \gamma c_t \epsilon_1 & 6A_{\text{SERCA}} \epsilon_1 & -3c_t^2 K A_{\text{SERCA}} \gamma^2 \epsilon_1^3 \\ 0 & 0 & -A_{\text{SERCA}} \epsilon_1 \end{pmatrix} \begin{pmatrix} \delta h_1 \\ \delta \epsilon_1 \\ \delta s_1 \end{pmatrix},$$

coupled to the equation

$$(A.35) \quad \epsilon_1' = 3A_{\text{SERCA}} \epsilon_1^2.$$

Invariance of the ϵ_1 -axis guarantees that the vector $(0, 1, 0)^T$ is tangent to \mathcal{M}_1 at both P and Q . By Lemma A.13, a second (linearly independent) tangent vector at P is given by $(-K_h^4 \rho_1^2, 0, 1)^T$. This gives an initial value problem for the variational equations (A.34) coupled to (A.35) with

$$\delta h_1(\rho_1) = -K_h^4 \rho_1^2, \quad \delta \epsilon_1(\rho_1) = 0, \quad \delta s_1(\rho_1) = 1.$$

Integrating equation (A.35), we obtain

$$\epsilon_1(t_1) = \frac{\rho_1}{1 - 3\rho_1 A_{\text{SERCA}} t_1},$$

from which we obtain the following expression for the time T taken for solutions to reach point Q :

$$T = \frac{1 - \rho_1 \beta_2}{3\rho_1 A_{\text{SERCA}}}.$$

Plugging the expression for $\epsilon_1(t_1)$ into (A.34), solving the initial value problem and evaluating it at T yields the desired result. \square

The map $\pi_{4,1} : \Sigma_{4,1} \rightarrow \Sigma_{4,2}$. Hyperbolic transition near p_s . We consider the dynamics near the hyperbolic equilibrium p_s in chart \mathcal{K}_2 , for which

$$\Sigma_{4,1} = \{(h_2, \beta_2, s_2) : |h_2| \leq \beta_2 \alpha_2, s_2 \in [0, \tilde{\rho}_4]\},$$

and

$$\Sigma_4 = \Sigma_{4,2} = \{(h_2, r_2, \beta_2) : |h_2| \leq \tilde{\alpha}_4, r_2 \in [0, \tilde{\rho}_4]\},$$

where $\tilde{\rho}_4 := \rho_3/\beta_2$ and $\tilde{\alpha}_4 := \alpha_2/\beta_2$. Noting that $\psi_2(0, 0, 0) = -A_{\text{SERCA}} < 0$, we may consider the system obtained from (A.31) after dividing the right hand side by a locally positive factor of $-\bar{\psi}_2(h_2, r_2, s_2)$:

$$(A.36) \quad \begin{aligned} h_2' &= -2h_2 - r_2 \left(\frac{\bar{\psi}_2(h_2, r_2, s_2)}{\psi_2(h_2, r_2, s_2)} \right), \\ r_2' &= -3r_2, \\ s_2' &= 2s_2. \end{aligned}$$

Like (A.31), system (A.36) has a hyperbolic saddle at $p_s = (0, 0, 0)$.

LEMMA A.15. *Given $\alpha_2, \beta_2, \tilde{\alpha}_4, \tilde{\rho}_4 > 0$ sufficiently small, the transition map $\pi_{4,1}$ is C^1 -smooth with form*

$$(A.37) \quad \pi_{4,1} : (h_2, \beta_2, s_2) \mapsto \left(O \left(\frac{h_2 s_2}{\beta_2} \right), \beta_2 \left(\frac{s_2}{\beta_2} \right)^2, \beta_2 \right).$$

Proof. Consider a solution $(h_2, r_2, s_2)(t)$ for (A.36) which satisfies

$$(h_2, r_2, s_2)(0) = (h_{1,in}, \beta_2, s_{2,in}), \quad (h_2, r_2, s_2)(T) = (h_{2,out}, r_{2,out}, s_{2,in}, \beta_2).$$

Direct integration yields $r_2(t) = \beta_2 e^{-3t}$ and $s_2(t) = s_{2,in} e^{2t}$, which leads to an expression for the transition time

$$T = \frac{1}{2} \ln \left(\frac{\beta_2}{s_{2,in}} \right),$$

proving that the transition map $\pi_{4,1}$ is of the form

$$\pi_{4,1} : (h_{2,in}, \beta_2, s_{2,in}) \mapsto \left(h_{2,out}, \beta_2 \left(\frac{s_{2,in}}{\beta_2} \right)^2, \beta_2 \right).$$

The estimate for $h_{2,out}$ in (A.37) follows by an application of Belitskii's theorem [2], see also [14, Theorem 3.1], which guarantees a C^1 transition of the desired form. \square

A.4.2. Proof of Lemma A.6. By Lemmas A.13, A.14, A.15, the restricted map π_{3,R_3} is C^1 since it is a restriction of a composition of the C^1 maps $\pi_{3,i}$ and $\pi_{4,i}$, $i = 1, 2$. Statements (ii) and (iii) in Lemma A.6 follow from Lemmas A.13, A.14, A.15, with strong contraction due to the map $\pi_{3,1}$.

Smoothness properties of the curve σ_4 in statement (i) follow from the fact that π_{3,R_3} is C^1 , and the fact that σ_4 is tangent to $r_1 = 0$ follows if we consider the expression for the tangent vector t_Q in (A.33) as a first order approximation of the curve $\mathcal{M} \cap \Sigma_{4,1}$ and apply the map $\pi_{4,1}$ in Lemma A.15.

Appendix B. Onset of oscillations.

Here, we briefly address the basic mechanisms leading to the onset of oscillations under parameter variation. We focus on three important model parameters: total calcium concentration c_t , the IP₃ concentration p and the time-scale parameter τ_{\max} of the h -dynamics.

B.1. Singular Andronov-Hopf bifurcation and canard explosion under variation of c_t or p . The first mechanism involves a singular Andronov-Hopf (AH) bifurcation and a corresponding *canard explosion* [8, 27, 29] and may arise in system (5.1) under variation in either p or c_t (but not under variation of τ_{\max}). The occurrence of this mechanism is correlated with the passage of the equilibrium q through the fold point F in Figure 6 under parameter variation. Note, that this implies a violation of the regularity condition (5.22). Results in [27, 8] then imply the existence of a nearby singular AH bifurcation for a locally unique parameter value $p = p_{ah} + O(\delta)$ or $c_t = c_{t,ah} + O(\delta)$. We highlight that periodic orbits arising from the singular AH bifurcation are expected to have an oscillation period $\mathcal{T} = O(\epsilon^{-7/4})$, which is intermediate between the intermediate-slow and infra-slow time-scales $t_1 = \epsilon^{3/2}t$ and $\tau_1 = \epsilon^2 t$ respectively.

Figure 11 shows a bifurcation diagram for system (5.1) under variation of c_t , with $p = 0.015$ and other parameters as in Table 3. As expected, the onset of oscillations happens via a singular AH bifurcation, at $c_t \approx 0.96$. The AH bifurcation is observed to be subcritical; the criticality has been confirmed numerically in MatCont [7] by showing that the corresponding first Lyapunov coefficient of the AH bifurcation is positive.

The rapid onset of the (non-standard) relaxation oscillations described in Theorem 5.9 is expected to occur over an exponentially small interval in c_t (or p); this is referred to as a *canard explosion* [8, 27, 19] because of the dramatic (or explosive) growth of amplitude. The rapid onset of oscillations is observed as an almost vertical segment in Figure 11.

Remark B.1. Due to the subcritical nature of the singular AH bifurcation observed in Figure 11, there exists a small parameter regime in which there is bistability between a stable relaxation/canard cycle and a stable equilibrium; on the scale of Figure 11, this regime is too small to be seen. The existence of this regime of bistability implies the occurrence of a saddle-node bifurcation of canard cycles (not indicated in Figure 11). We refer to, e.g., [27, 6] for details.

Figure 12 shows another bifurcation diagram for system (5.1) under variation of c_t , this time with all parameters as in Table 3. Note the S-shaped branch of equilibria which indicates that the choice of $p = 0.025$ puts the system into the regime in which there can be three equilibria; see Figure 7. There is a subcritical singular AH bifurcation at $c_t \approx 0.63$. As before, the criticality has been confirmed numerically in MatCont

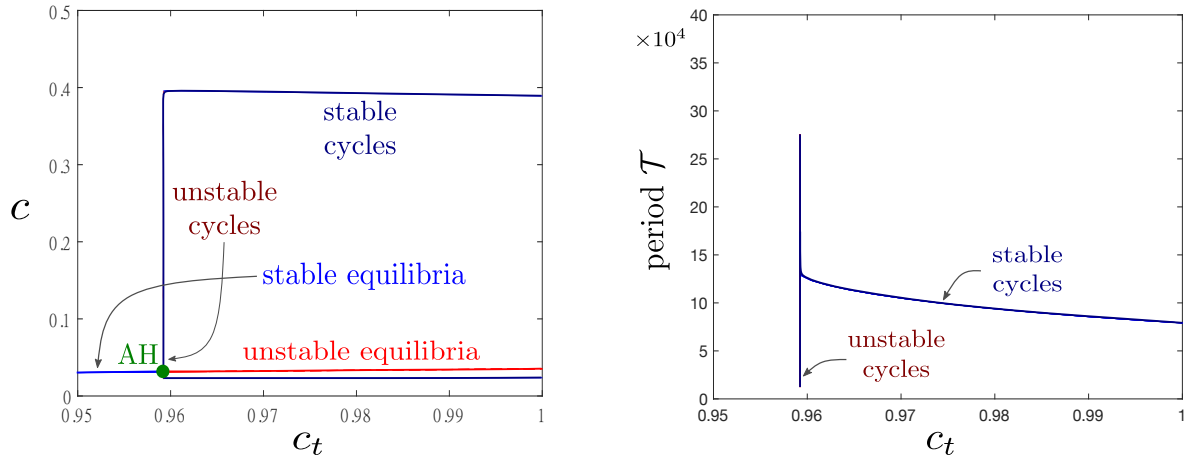


Fig. 11: Bifurcation diagram for system (5.1) under variation of c_t , computed numerically in MatCont [7], for $p = 0.015$ and other parameters as in Table 3: (Left) The onset of oscillations happens via a subcritical singular Andronov-Hopf (AH) bifurcation at $c_t \approx 0.96$. The transition to stable relaxation oscillations happens via a canard explosion in an exponentially small parameter regime. (Right) Period of the branch of relaxation oscillations.

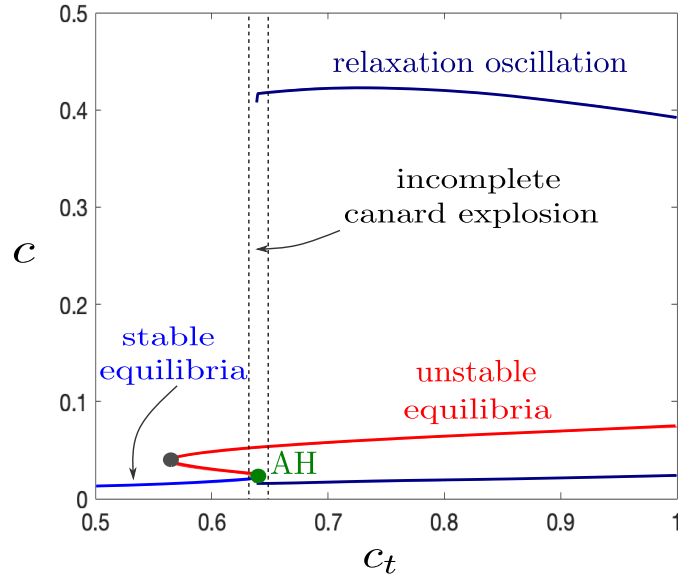


Fig. 12: Bifurcation diagram for system (5.1), computed numerically in MatCont [7] with parameters as in Table 3; compare with Figure 11. A subcritical singular AH bifurcation occurs on the middle branch of the S-shaped curve of equilibria. Theoretical considerations [6] lead us to expect this AH bifurcation to produce a short unstable branch of periodic orbits but we were unable to find this numerically because of the extreme stiffness of the system. The transition to stable relaxation oscillations is similarly expected to happen via an ‘incomplete’ canard explosion involving multiple singular bifurcations and canard homoclinic cycles; see, e.g., [6] for details.

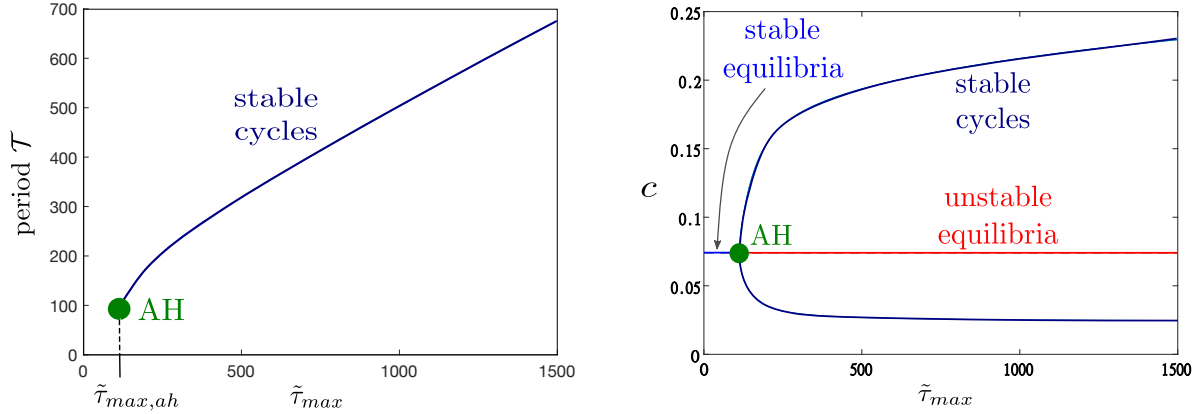


Fig. 13: Bifurcation diagrams for (5.1) as a function of $\tilde{\tau}_{\max}$, calculated with MatCont [7] for parameter values as in Table 3: (Left) Period \mathcal{T} as a function of $\tilde{\tau}_{\max}$; (Right) Maximum and minimum values of c as a function of $\tilde{\tau}_{\max}$. Note that we plot with respect to $c = \sqrt{\epsilon}C$ here. The green disk indicates the onset of oscillations at a supercritical AH bifurcation at $\tilde{\tau}_{\max} = \tilde{\tau}_{\max,ah} \approx 112.5$ or equivalently, $\nu_{\max,ah} \approx 5.83 \times 10^{-2}$.

[7]. Importantly, the singular AH bifurcation resides on the middle branch (close to the lower fold) of the S-shaped equilibrium branch.

The details of the canard explosion in system (5.1) can differ quite significantly, depending on the number of equilibria. In the case that there are three equilibria, there is an *incomplete canard explosion* in which canard cycles may terminate prematurely in a homoclinic bifurcation. Figure 12 indicates the small zone where such an incomplete canard explosion happens. In this zone, the large relaxation oscillations turn into large canard cycles which terminate in a large amplitude homoclinic bifurcation. Similarly, the small unstable oscillation cycles born out of the singular AH bifurcation turn into small canard cycles that terminate in a small amplitude homoclinic bifurcation.

Remark B.2. A rigorous treatment of this incomplete canard explosion goes beyond the scope of this article and is deferred for future work. We refer to, e.g., [6], which studies that phenomenon in the context of (neural) excitation.

B.2. Regular Andronov-Hopf bifurcation under τ_{\max} variation. From a physiological point of view, τ_{\max} is an important parameter, as it is one of the major determinants of oscillation period. For example, although we do not have a detailed understanding of oscillation frequency as a function of τ_{\max} , we do know that an increase in τ_{\max} leads to a decrease in oscillation frequency [45]. Numerical studies of the corresponding open-cell model (3.2) in [45] showed the onset of relaxation oscillations via a supercritical Hopf bifurcation as τ_{\max} is increased. These findings have been reproduced for system (5.1) in Figure 13, which shows the period of oscillations in system (5.1) as a function of the original dimensionless quantity $\tilde{\tau}_{\max}$ from Section 4. We revert to the original $\tilde{\tau}_{\max}$ in these figures and the following in order to consider parameter variations over several orders in ϵ .

In order to identify the AH bifurcation analytically, we consider system (5.9) except with

$$(B.1) \quad \tau_{\max} = \delta \nu_{\max} = \epsilon^{1/2} \nu_{\max},$$

and vary $\nu_{\max} \in [0, \xi]$, where $\xi > 0$ is fixed, as a bifurcation parameter. The alternative scaling (B.1) amounts to restriction to the scaling regime $\tilde{\tau}_{\max} = O(\epsilon^{-3/2})$, instead of the scaling regime $\tilde{\tau}_{\max} = O(\epsilon^{-2})$ corresponding to relaxation oscillations. In this case, the dynamics within regime (R2) are governed by

$$(B.2) \quad \begin{aligned} h' &= -\frac{1}{\tau_h(C)} (h - h_\infty(C)), \\ C' &= \tilde{f}_0(h, C) + \delta \tilde{f}_{\text{rem}}(h, C, \delta). \end{aligned}$$

System (B.2) is similar to system (5.9), except that there is no small parameter factoring the equation for h' . Setting $\delta = 0$ in (B.2) yields

$$(B.3) \quad \begin{aligned} h' &= -\frac{1}{\tau_h(C)} (h - h_\infty(C)), \\ C' &= \tilde{f}_0(h, C), \end{aligned}$$

which has equilibria for (h_*, C_*) satisfying $h_* = h_\infty(C_*) = \zeta(C_*)$, where $\zeta(C)$ is given by (5.13). In fact, it follows from our observations in Section 5.2 that system (B.3) can have one, two, or three equilibria, depending on the location in (p, c_t) -parameter space. We note that system (B.2) is a *regular perturbation problem*, with leading order dynamics determined by the limiting system (B.3).

The observed AH bifurcation is described in the following result. Note that neither $h_\infty(C)$ nor $\zeta(C)$ depend on $\tilde{\tau}_{\max}$, so the number and location of equilibria is also independent of $\tilde{\tau}_{\max}$.

THEOREM B.3. *Consider system (B.3), with a unique equilibrium $q = (h_*, C_*)$ such that*

$$(B.4) \quad C_* > C_F, \quad |D_C h_\infty(C_*)| > \frac{D_C \tilde{f}_0(q_\delta)}{D_h \tilde{f}_0(q_\delta)},$$

where the coordinate C_* can be written explicitly in terms of the model parameters. Then there exists $\delta_0 > 0$ such that for each $\delta \in [0, \delta_0)$, system (B.2) has a unique equilibrium q_δ such that $q_\delta \rightarrow q$ as $\delta \rightarrow 0$. Furthermore, q_δ undergoes an AH bifurcation for

$$(B.5) \quad \nu_{\max, \text{ah}}(\delta) = \frac{(K_h^4 + C_*^4) C_*}{2A_{\text{SERCA}} K_h^4 (C_*^2 - 2K\gamma^2 c_t^2)} + O(\delta),$$

or, equivalently,

$$\tilde{\tau}_{\max, \text{ah}}(\epsilon) = \epsilon^{-3/2} \nu_{\max, \text{ah}}(\sqrt{\epsilon}) = \frac{(K_h^4 + C_*^4) C_*}{2A_{\text{SERCA}} K_h^4 (C_*^2 - 2K\gamma^2 c_t^2)} \epsilon^{-3/2} + O(\epsilon^{-1}).$$

Proof. The fact that C_* can be written explicitly in terms of the model parameters follows from the fact that C_*^2 is a solution to the cubic polynomial (5.19).

Equilibria of system (B.2) satisfy $\tilde{f}_0(h, C) + \delta \tilde{f}_{\text{rem}}(h, C, \delta) = 0$. For $\delta = 0$ in particular we have $\tilde{f}_0(\zeta(C), C) = 0$ and $D_h \tilde{f}_0(\zeta(C), C) > 0$ for all $C > 0$, recalling the expressions in (5.11). It follows by the implicit function theorem that there exists an open interval U , a constant $\tilde{\delta}_0 > 0$ and a smooth function $\varphi : U \times [0, \tilde{\delta}_0) \rightarrow \mathbb{R}$ such that for all $(C, \delta) \in U \times [0, \tilde{\delta}_0)$ we have

$$\tilde{f}_0(\varphi(C, \delta), C) + \delta \tilde{f}_{\text{rem}}(\varphi(C, \delta), C, \delta) = 0,$$

where $\varphi(C, \delta) = \zeta(C) + \delta \psi(C, \delta)$ for a smooth function ψ . Evaluating the Jacobian J at q_δ yields trace

$$\text{Tr} J(q_\delta) = -\frac{1}{\tau_h(C_*)} + D_C \tilde{f}_0(q_\delta) + \delta \tilde{f}_{\text{rem}}(q_\delta, \delta),$$

and determinant

$$(B.6) \quad \det J(q_\delta) = -\frac{1}{\tau_h(C_*)} \left(D_C \tilde{f}_0(q_\delta) + D_C h_\infty(C_*) D_h \tilde{f}_0(q_\delta) \right) + O(\delta).$$

Since we assume that $C_* > C_F$, the inequalities $D_C \tilde{f}_0(q_\delta) > 0$ and $D_h \tilde{f}_0(q_\delta) > 0$ follow by equations (5.14) and (5.16). Since $D_C h_\infty(C_*) < 0$ follows by direct calculations, the determinant condition $\det J(q_\delta) > 0$ follows by the second condition in (B.4) for all δ sufficiently small. Finally, the Andronov-Hopf condition $\text{Tr} J(q_\delta) = 0$ can be solved for $\delta \in [0, \delta_0)$, $\delta_0 > 0$ sufficiently small, using the implicit function theorem. We obtain

$$(B.7) \quad \nu_{\max, \text{ah}}(\delta) = \frac{K_h^4 + C_*^4}{K_h^4 D_C \tilde{f}_0(\zeta(C_*), C_*)} + \delta w(C_*) + O(\delta^2),$$

where

$$(B.8) \quad w(C_*) = 4A_{\text{IPR}}\gamma c_t C_*^3 \psi(C_*, 0) - 5A_{\text{IPR}}C_*^4 \zeta(C_*) - 2KA_{\text{SERCA}}\gamma^2 c_t.$$

The function $\psi(C_*, 0)$ can be approximated by standard matching techniques in order to obtain an explicit higher order correction, but we omit this calculation for brevity. Expression (B.5) follows from (B.7) after substituting the expression in (5.14) for $D_C \tilde{f}_0(\zeta(C_*), C_*)$. \square

Numerical observations indicate a supercritical bifurcation and hence, the existence of nearby stable oscillations; see Remark B.4 below. The qualitative shape of the profile in Figure 13 can also be explained by our findings. Let \mathcal{T} denote the oscillation period on the fastest time-scale t , as in Proposition 5.11. Then

- (i) The fixed point analysis used to prove Theorem B.3, in particular the form of the determinant (B.6), implies an oscillation period $\mathcal{T} \propto \epsilon^{-3/2} \sqrt{\nu_{\text{max}}} = \epsilon^{-1/2} \sqrt{\tilde{\tau}_{\text{max}}}$ for parameter values $\tilde{\tau}_{\text{max}} = O(\epsilon^{-3/2})$ close to the AH bifurcation.
- (ii) Proposition 5.11 implies an oscillation period $\mathcal{T} = O(\epsilon^{-2})$ and leading order dependence $\mathcal{T} \propto \tilde{\tau}_{\text{max}}$ for parameter values $\tilde{\tau}_{\text{max}} = O(\epsilon^{-2})$, in the relaxation oscillatory regime.

Remark B.4. The conditions for the applicability of Theorem B.3 are satisfied for system (B.2) with parameter values taken from Table 3 and $\delta = \sqrt{2.5 \times 10^{-3}} = 5 \times 10^{-2}$. The conditions in (B.4) are satisfied since

$$|D_C h_\infty(C_*)| \approx 0.20 > \frac{D_C \tilde{f}_0(q_\delta)}{D_h \tilde{f}_0(q_\delta)} \approx 8.3 \times 10^{-2},$$

and the AH bifurcation occurs at $q_\delta = (h_*, C_*) \approx (0.0792, 1.48)$, so $C_* > C_F \approx 0.68$. We obtain a numerical estimate of $\nu_{\text{max,ah}} \approx 5.83 \times 10^{-2}$, in close agreement with the leading order estimate (B.5) as $\delta \rightarrow 0$:

$$\nu_{\text{max,ah}}(0) = \frac{(K_h^4 + C_*^4) C_*}{2A_{\text{SERCA}} K_h^4 (C_*^2 - 2K\gamma^2 c_t^2)} \approx 5.42 \times 10^{-2},$$

where we have used the numerical value for C_* . A first Lyapunov coefficient $l_1 \approx -3.13 < 0$ was calculated numerically in the software package MatCont [7], indicating a supercritical bifurcation.